

**A 16X16 Basic-Cell High Speed Silicon Germanium Field  
Programmable Gate Array**

by

Peng Jin

A Thesis Submitted to the Graduate  
Faculty of Rensselaer Polytechnic Institute  
in Partial Fulfillment of the  
Requirements for the degree of  
Master of Science  
Major Subject: Electrical Engineering

Advisor:

---

John F. McDonald, Thesis Advisor

Rensselaer Polytechnic Institute  
Troy, New York  
November, 2007  
(For Graduation December 2007)

# CONTENTS

CONTENTS.....	I
LIST OF TABLES.....	III
LIST OF FIGURES.....	IV
ACKNOWLEDGMENT.....	VII
ABSTRACT.....	III
1. Introduction.....	1
1.1 Research History.....	1
1.2 Thesis Outline.....	3
2. FPGA and XC6200 Architecture.....	4
2.1 FPGA.....	4
2.2 Xilinx 6200 Field Programmable Logic Array.....	6
3 Silicon Germanium (SiGe) Proces.....	13
3.1 SiGe HBT Process Overview.....	13
3.2 Performance Advantage.....	15
3.3 Graded Base HBT.....	15
3.4 IBM SiGe Proces.....	16
3.5 Current Mode Logic (CML) .....	19
3.6 Difficulties of designing a CML high speed FPGA.....	24
4 Large Scale (16 x16 BC array) SiGe FPGA design.....	25
4.1 The XC 6200 Basic Cell.....	25
4.2 Voltage Controlled Oscillator (VCO) in SiGe FPGA.....	32
4.3 Input multiplexer block, output selection blocks and FPGA core.....	34
4.4 Programming scheme in the Basic Cell and FPG.....	34
4.5 Power Rails design.....	38
4.6 Clock and programming circuit clock distributions.....	41
4.7 SiGe FPGA Basic Cell Configuration.....	45
4.8 Programming the Basic cell array.....	50
4.9 Pin assignments of the 16 x 16 FPGA.....	52

4.10 layout, programming sequence and power consumption.....	53
5 the 16 x 16 SiGe FPGA Test and a New Chip Design.....	56
5.1 the 16 x 16 FPGA chip test.....	56
5.2 16 x 16 SiGe FPGA Test Results.....	61
5.3 the New 16 x 16 FPGA chip design.....	65
5.4 Future work.....	65
REFERENCE.....	67

## LIST OF TABLES

Table 2.1 XC6200 family.....	7
Table 2.2 Function Derivation Table of the BCI.....	12
Table 3.1 HBT comparison for 0.5 $\mu\text{m}$ , 0.25 $\mu\text{m}$ , and 0.18 $\mu\text{m}$ generations.....	13
Table 3.2 Equations of the CML buffer.....	21
Table 3.3 Performance of the SiGe CML.....	22
Table 4.1 Dynamic Routing Power Usage. ....	31
Table 4.2 Characteristics of the metal layers of the IBM 7 HP process.....	39
Table 4.3 Equations for calculating power droop and power rail width.....	39
Table 4.4 Control signals of the input MU.....	46
Table 4.5 Configuration of the input MUX: X1, X2 and X3. ....	47
Table 4.6 Selection of the combinational and sequential operation.....	47
Table 4.7 Selection of the CLB combinational or sequential outputs. ....	48
Table 4.8 Configuration of the MUX of Output Routing Stage. ....	48
Table 4.9 Bit pattern of the Basic Cell.....	49
Table 4.10 Estimated power consumption of the different Basic Cell configurations .....	55

## LIST OF FIGURES

Figure 2.1 Structure of an FPGA.....	6
Figure 2.2 XC6200 FPGA accelerates DSP application block.....	7
Figure 2.3 Schematic of the XC6200 Basic Cell.....	8
Figure 2.4 Schematic of the Function Unit in the XC6200 Basic Cell.....	9
Figure 2.5 Connections between neighboring Basic Cells.....	9
Figure 2.6 4x4 cell block and Length 4 FastLANEs.....	10
Figure 2.7 Connections between 4x4 blocks (16x16 block).....	11
Figure 2.8 Function Unit of XC6200.....	11
Fig. 3.1 IBM foundry SiGe BiCMOS technology roadmap.....	14
Figure 3.2 Energy band diagram for Si BJT and graded-base SiGe both biased in forward active mode at low injection. ....	15
Figure 3.3 Ge content design trade-off .....	16
Figure 3.4 Cutoff frequencies of several SiGe Technologies.....	17
Figure 3.5 $f_T$ vs. $I_C$ curve for IBM SiGe 7HP technolog.....	17
Figure 3.6 Max. Switching frequency versus power consumption of CML and ECL logic.....	20
Figure 3.7 A conventional CML Buffer.....	21
Figure 3.8 Transfer characteristics of the CML buffer at different values of $\beta$ .....	22
Figure 3.9 CML D-latch configuration with two input levels. ....	23
Figure 3.10 Propagation delay of the CML buffer with the emitter size of 0.2 x 0.64 $\mu\text{m}$ .....	23
Figure 4.1 Block diagram of the 16 x 16 array FPGA.....	25
Figure 4.2 XC6200 Basic Cell .....	26
Figure 4.3 Redesigned input routing block. ....	27
Figure 4.4 General form of the new MUX design. The new input routing stage has 4:1 and 5:1 MUXs and the new output routing stage has 4:1 MUXs.....	27
Figure 4.5 Latch 1 in the new D-FF design.....	28

Figure 4.6 Latch 2 in the new D-FF design.....	29
Figure 4.7 Schematic of the BCII. ....	29
Figure 4.8 Layout of the Basic Cell.....	30
Figure 4.9 Layout of the new Basic Cell.....	31
Figure 4.10 the VCO's architecture. ....	32
Figure 4.11 Schematic of the VCO buffer.....	33
Figure 4.12 Layout of the VCO buffer Figure 4.12 Layout of the VCO buffer. ....	33
Figure 4.13 Block diagram of the input/output blocks and the FPGA core. ....	33
Figure 4.14 Schematic of the programming scheme with clock distribution. ....	35
Figure 4.15 Layout of 42 SRAM cells. ....	35
Figure 4.16 Layout of 42 bits shift register.....	35
Figure 4.17 Simulation of the 42-bit memory.....	36
Figure 4.18 Simulation result of the shift register output with input data period of 800 ps.....	36
Figure 4.19 Block diagram of an array of basic cells with programming circuits connected. ....	37
Figure 4.20 Programming and memory circuits in the SiGe FPGA. ....	37
Figure 4.22 Simplified circuit model of the power distribution. ....	38
Figure 4.23 (a) Vcc (GND) power rail in the Basic Cell.. (b) Vee (-2.8 V) power rail of the Basic Cell. ....	40
Figure 4.24 Clock tree of the 8x8 array as an example in the FPGA core. ....	40
Figure 4.25 Schematic (a) and layout (b) of the clock repeater.....	41
Figure 4.26 Test structure of the repeater driving capability. ....	42
Figure 4.27 Simulation result of the clock repeater driving 400~700 $\mu$ m wire loads with the 10 GHz test signal. ....	42
Figure 4.28 Simulation result of the clock repeater loaded with one to five clock repeater loads. ....	42
Figure 4.29 Propagation delay between A, B, C and D in clock tree shown in Figure 4.30. ....	43
Figure 4.30 Clock distribution of the SiGe FPGA.....	43

Figure 4.31 Detail clock distribution circuit in the 4 x 4 BC array.....	44
Figure 4.32 Schematic of the BCII. ....	45
Figure 4.33 Schematic of the MUXs in the input routing stage of a BC. ....	46
Figure 4.34 Configuration of the MUX based in the Output Routing Stage. ....	48
Figure 4.35 Configuration data path in the 4x4 BC array.....	51
Figure 4.36 Block diagram and data stream path of the 8 x 8 BC array. ....	51
Figure 4.37 Programming Circuit. ....	52
Figure 4.38 Pin arrangement of the 16-pin probe used in the 16 x 16 SiGe FPGA...53	
Figure 4.39 Pin arrangement of the 10-pin power probe used in the 16 x 16 FPGA.....	53
Figure 4.40 16 x 16 FPGA array programming structure. ....	54
Figure 4.41 Timing diagram of the SiGe FPGA.....	54
Figure 5.1 Pseudorandom binary sequences. ....	56
Figure 5.2 Schematic of a four bit linear feedback sequences register (LFSR). ....	56
Figure 5.3 Test circuitry of the 16 x 16 SiGe FPGAHigh speed input and output signals.....	57
Figure 5.4 Pin assignment of the high speed (> 10 GHz) signals. ....	58
Figure 5.5 Input / Output arrangement of the programming data. ....	59
Figure 5.6 Schematic of the tapered buffer driving a 180 $\mu\text{m}$ wire. ....	59
Figure 5.7 Pin assignment of the low speed (> 1 GHz) inputs and outputs.....	60
Figure 5.9 Test blocks on programming the SiGe FPGA configuration with an FPGA board.....	61
Figure 5.10 8-stage Ring Oscillator Test Circuitry.....	62
Figure 5.11 8-stage Ring Oscillator Test Result.....	62
Figure 5.12 2-stage Ring Oscillator Test circuitry. ....	63
Figure 5.13 2-stage Ring Oscillator Test Result.....	64

## **ACKNOWLEDGMENT**

I would like to thank my advisor Professor John F. McDonald for his great support and advice through out my Master program at Rensselaer. Prof. McDonald gave me the opportunity to be working with the latest technologies on this SiGe FPGA project together with some great ideas and suggestions on both the project and my study life at RPI. He is kind to all his students and keeps working every day for our current projects and group's future. I really appreciate what he did for us.

I would like to thank Professor Russell P. Kraft and Steve Nicolas for the great help on the whole process of my chip test.

My group members always support me by kinds of methods. Dr. Jong-ru Guo designed the first working FPGA chip, and was still concerned about the project even after he graduated. Michael Chu, and Dr. Okan Erdogan did a great help on my design and test. Dr. Young Yim and Jimwoo Kim are always there when I need their help. Philip Jacob and Aamir Zia are two good friends to talk with on any technical questions.

Finally I would like to thank my Family and friends for keeping motivated while I pursued a long academic program.

## ABSTRACT

The Field Programmable Gate Array (FPGA) is a configurable circuit consisting of logic blocks surrounded by a programmable routing structure. The routing cells and logic cells are programmed by memories whose data is provided by the configuration file of the CAD software to perform the desired functions. The first FPGA was introduced by Xilinx in 1985. Since then, FPGAs have become denser, cheaper and much more powerful in terms of performance and functionality than before. However, because FPGAs utilize switches to route signals to their neighbor circuits and the routing CMOS switches introduce more delay to the FPGA, thus reducing the overall performance, the operating frequency of the current commercial FPGAs has not increased as fast as the operating frequency of current ASICs.

As high-speed systems are becoming more mature, the need for high speed reconfigurable systems is more urgent. But In order to improve the performance of an FPGA, many methods have been proposed. In the SiGe FPGA project, Silicon Germanium (SiGe) Heterojunction Bipolar Transistor (HBT) and Current Mode Logic (CML) are used to enhance the overall speed of the Basic Cell (BC) of the FPGA to compensate the performance reduction caused by interconnect wires and routing switches.

After successfully designing several FPGA chips with special programmed functions to test the performance of the basic cell, a large scale SiGe FPGAs has been designed and fabricated which contains a 16 x 16 Basic Cell array. The design methodology of Basic Cell, power rail, clock distribution and Voltage Control Oscillator (VCO) are included. Measured results showed its operating frequency can reach 12 GHz. Based on this design, a new version of 16 x 16 Basic Cell FPGA was fabricated with several functions updated and ready to test.

# **Introduction**

## 1.1 Research History

Field Programmable Gate Arrays (FPGAs) have been popular since 1988 when the first FPGA was introduced by Xilinx. Briefly, the development of FPGAs leads to two different objectives. The first seeks to improve the FPGA's performance, functionality and reliability. The other targets a reduction in the cost, power consumption and size of the FPGA.

As the circuit operating frequency increases towards the GHz range, the need for a high speed configurable function increased. However, interconnect switches between configurable cells limit the operating frequency of most commercial FPGAs. The demand for high speed FPGAs has always been on the rise. People were only able to achieve frequencies in the range of 10-500 MHz using CMOS. There are few commercial FPGAs with operating frequency running to gigahertz (GHz) range. Xilinx has just proposed in their Virtex-5 FPGA an operating frequency only as high as 1.25 GHz. Even that frequency is limited to the Input Output Block (IOB). The availability of SiGe HBT devices has opened the door for Gigahertz FPGAs. The integration of these high-speed SiGe HBTs and low power CMOS gives a significant speed advantage to SiGe FPGAs compared to traditional CMOS FPGAs.

A new FPGA design was proposed by Dr. Bryan Goda In 2000, which took advantage of the high speed switching characteristics of the Silicon Germanium (SiGe) Heterojunction Bipolar Transistor (HBT) and the low output swing voltage of Current Mode Logic (CML) designs to enhance the performance of the FPGA into the GHz range. The propagation delay of the reconfigurable cell has been greatly reduced compared to the CMOS competitors. However, the power consumption of CML is too large since current flows constantly in a logic tree. The overall power consumption and the number of the CML cells in the FPGA limit the FPGA from scaling up.

There are methods to alleviate the expected problems from the large power consumption. The first is to reduce the current flowing in the CML to reduce its static power consumption. Another is to reduce the logic elements used in a configurable cell by merging their functions together. Lastly, unused circuits can be powered down.

In early 2001, Dr. Jong-Ru Guo came up with a “single level” current tree method to implement multiplexers. The new multiplexer had several features. For example, the multiplexer can be turned off entirely and multiplexers of any number inputs can be implemented. Based on this idea, the author introduced a Multi-Mode Routing method to turn off unused basic cells and circuits. Much power is saved by using this new routing method.

In late 2001, Dr. Chao You, introduced a new basic cell structure, which has been proven to enhance the performance by 40% and reduce 30%-70% total power consumption. This is the major contribution to the research group by this thesis. The new structure has more routing capability, less gate delays and requires less power supply voltage. It also preserves all the original functions listed in the XC6200 datasheet.

Starting in May 2002, the FPGA research group fabricated several chips using this new basic cell structure to prove the performance achievements. The first FPGA chip configured as a ring oscillator, in May 2002, achieved the expected enhanced functionality, and at the same time, the gate delay was as low as 100 ps per cell. The measurement results were published in *Microprocessors and Microsystems*. The second FPGA chip configured as a 4-channel demultiplexer, in Nov 2003, revealed that the sequential logic operation clock could be as high as 11 GHz.

A big FPGA chip with 20 x 20 basic cells and memory was fabricated and tested during 2005, but the result shows that was not working because the errors during the design steps. After fixing the errors, and checking with the new tools, Assura, which is much faster than the old one and therefore very helpful, a 16X16 basic cell FPGA was fabricated and tested soon during 2005 and 2006. The test results proved the chip can

run up to 12GHz.

The 16X16 basic-cell FPGA still has some disadvantages which did not allow people see the high speed signal directly from the oscilloscope, and limited the performance of the chip. The author fixed these problems and has a new 16X16 FPGA chip fabricated in 2007, and will test it soon.

## 1.2 Thesis Outline

This thesis is organized as follows. Chapter 1 is a simple introduction of the whole project and its history. Chapter 2 describes the history of bipolar FPGAs and explains in detail the XC6200 architecture. Chapter 3 explains why the Silicon Germanium (SiGe) process is chosen as the semiconductor process, and the advantages of Current Mode Logic (CML) family. Chapters 4 presents the details of the first working SiGe FPGA chip of this project, including how it was designed and some considerations. The test plan and the test result of this chip are provided in Chapter 5, together with a new chip designed and future work consideration.

## **2. FPGA and XC6200 Architecture**

### **2.1 FPGA**

#### **2.1.1 Introduction**

FPGA is considered to be a hybrid between Application Specific Integrated Circuits (ASICs) and programmable processors. One of the most fundamental tradeoffs is the balance between flexibility and efficiency. The ASICs, on one hand, contain circuitry dedicated to a particular set of tasks. It has the advantages of low power dissipation and high clock speeds, but at the cost of flexibility and a long “time to market”. ASICs become obsolete when the target application changes. On the other end of the spectrum are the general purpose (GP) processors. GP processors have a limited and fixed set of instructions. By breaking the functions into smaller pieces, it is possible to execute each function sequentially. However, in cases where the instruction sets are not well suited to the task at hand, the GP processors deliver relatively poor performance.

The FPGA is aimed at this problem space between ASICs and general-purpose processors. The goal of these reconfigurable architectures is to achieve implementation efficiency approaching ASICs, while providing the silicon reusability of general purpose processors. Unlike programmable processors where computations must be implemented as some sequence of available operations, FPGAs can be programmed to compute the problem in a spatial fashion.

#### **2.1.2 Current Commercial CMOS FPGAs**

At the current market, there are lots of FPGA vendors including Actel, Altera, Atmel, Cypress, Lattice, Lucent, Quicklogic, Triscend, and Xilinx, out of which Altera and Xilinx are currently the leading FPGA vendors.

The Programmable Logic Device (PLD) market is growing rapidly. Most current commercial FPGA products chose CMOS as the basic logic family because of its low power and easy implement. However, MOS gates are notorious for their low driving

capability, plus CMOS FPGAs use pass transistors as their programmable interconnect, and therefore the fastest CMOS FPGAs only operate in the MHz range. The use of pass transistors has prevented FPGAs from reaching higher speeds. In the FPGA, a pass transistor is turned ON or OFF by driving its gate to the top most voltage or lowest potential using a memory cell. The advantage of the pass transistor is its bi-directional signal propagation. However, it also comes with a large performance penalty due to its poor bandwidth. There are also some other programming technologies like antifuse, flash, EEPROM, etc. Antifuse provides significantly low ON resistance and capacitance relative to SRAMbased pass transistors. However, the programming cannot be reversed due to its non-volatility. The programming of flash and EEPROM can be removed, but it is more complex and time-consuming. There is no perfect programming technology for CMOS FPGAs at this time.

### **2.1.3 High Speed Applications**

High-speed high-precision computation is required for many digital signal processing, genome analysis, computer graphics and image processing applications. In many cases where high speed computation is not required, high speed FPGAs are still advantageous due to their ability to support larger systems without compromising speed. For example, in image processing applications, the spatial-domain two-dimensional (2-D) convolution is a computationally demanding operation under real time requirement. Software implementation of this has become a bottleneck for image processing applications. However, this algorithm presents a very high level of parallelism which is well suited to FPGA implementation. Although the clock speed of the FPGA is lower than the speed of the CPU, this parallelism can result in significant speedup.

Another example is the use of FPGAs for bioinformatics, such as DNA sequencing and protein sequence analysis. FPGAs can provide efficient implementation of bioinformatics algorithms. K.-P. Lam and S.-T. Mak have shown that the XCV800 FPGA implementation is 3063 times faster than using a PIII 450 MHz computer.

## 2.2 Xilinx 6200 Field Programmable Logic Array

A Field Programmable Gate Array (FPGA) is a configurable circuit consisting of logic blocks surrounded by a programmable routing structure. The structure is shown in Figure 2.1. The input signals (A, B and C) are routed through the Input/ Output (I/O) cells on three different sides to the routing cells, and then passed to the configurable

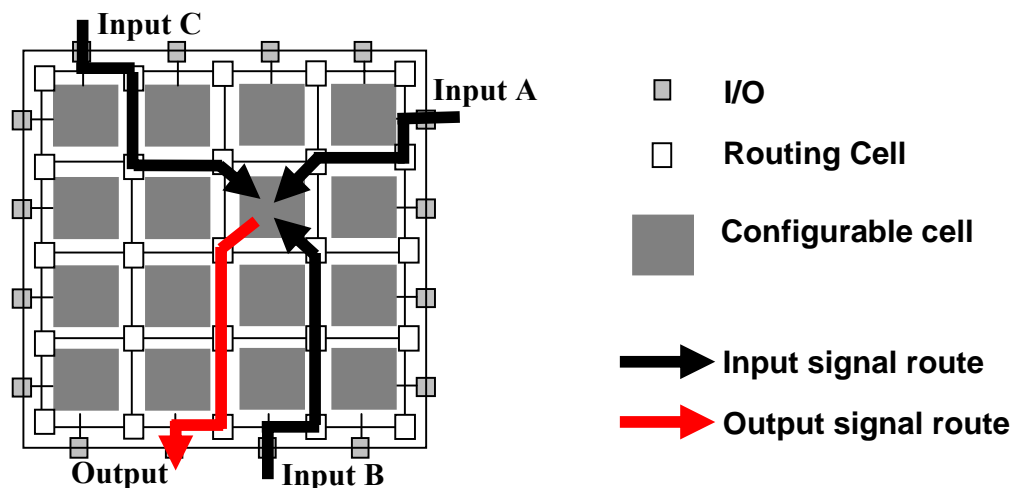


**Figure 2.1 Structure of an FPGA**

cells. The routing cells and logic cells are programmed by a memory (Static Random Access Memory, SRAM) whose data is provided by the configuration file generated from the CAD software to perform the desired functions. Currently, the versatility of the FPGAs has made them useful for networking applications, such as network routers, however the relatively low operating frequency of current commercial FPGAs limits their use in high frequency applications. The Xilinx 6200 FPGA was selected as the blueprint of the high speed FPGA design because of its open source structure and the availability of its programming software. Other structures can be implemented as the tools and related information becomes available.

### 2.2.1 Xilinx 6200 family

This project uses the Xilinx XC6200 as an initial starting point. The Xilinx 6200

family (XC6200) was developed around 1980 for co-processing in embedded DSP system applications as shown in Figure 2.2.

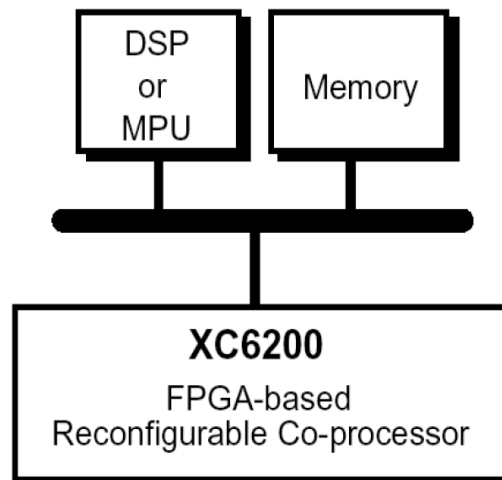


**Figure 2.2 XC6200 FPGA accelerates DSP application block**

The XC6200 is open-source in both hardware and software, which gives our design more resources to obtain design information from. The XC6200 is a multiplexer based FPGA, which can provide any combinational logic function if inputs are properly selected. Among other generally used functional blocks, such as NAND gates, Lookup Tables and AND-OR gates, a multiplexer based logic block has a shorter gate delay than other types. Another reason for choosing the XC6200 is that a multiplexer based FPGA can be converted to a CML circuit without losing much performance.

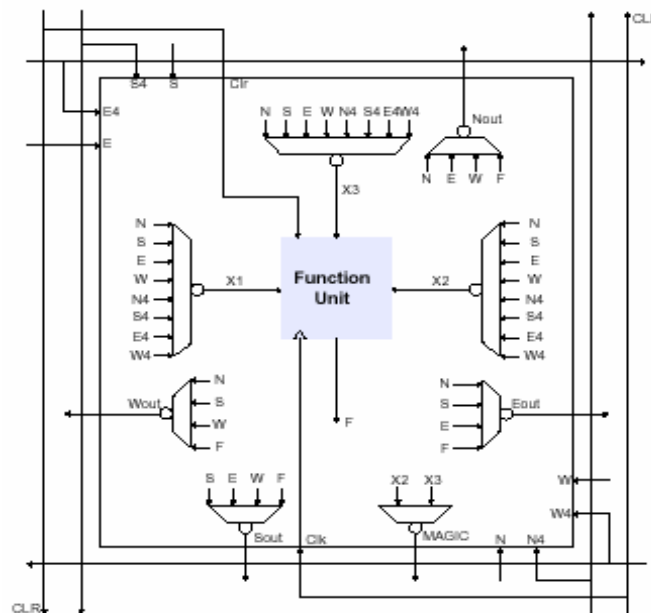
**Table 2.1 XC6200 family**

Device	<b>XC6209<sup>†</sup></b>	<b>XC6216</b>	<b>XC6236<sup>†</sup></b>	<b>XC6264</b>
Typical Gate Count Range	9000-13000	16000-24000	36000-55000	64000-100000
Number of Cells	2304	4096	9216	16384
Number of Registers	2304	4096	9216	16384
Number of IOBs	192	256	384	512
Cell Rows x Columns	48x48	64x64	96x96	128x128

These XC6200 family FPGAs were designed to operate in close cooperation with a microprocessor or microcontroller to provide an implementation of functions normally placed onto an Application Specific Integrated Circuit (ASIC) The XC6200 can provide high gate counts for data path or regular array type designs. Table 2.1 shows the number of the cells, registers and Input Output Blocks (IOBs) of the FPGAs in the XC6200 family.

The XC6200 has a large array of simple configurable cells called basic cells to implement different sets of logic functions. The XC6200 uses a simple, symmetrical, hierarchical and regular architecture that allows novice users to quickly make efficient use of the resources available. To achieve higher performance, it is specially designed for the high speed applications by using a simpler logic structure.

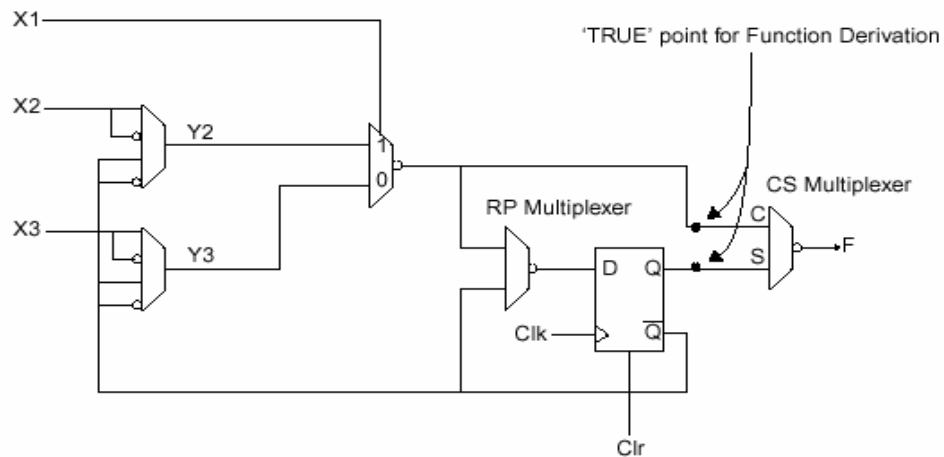
### 2.2.2 Structure of the Configurable cell



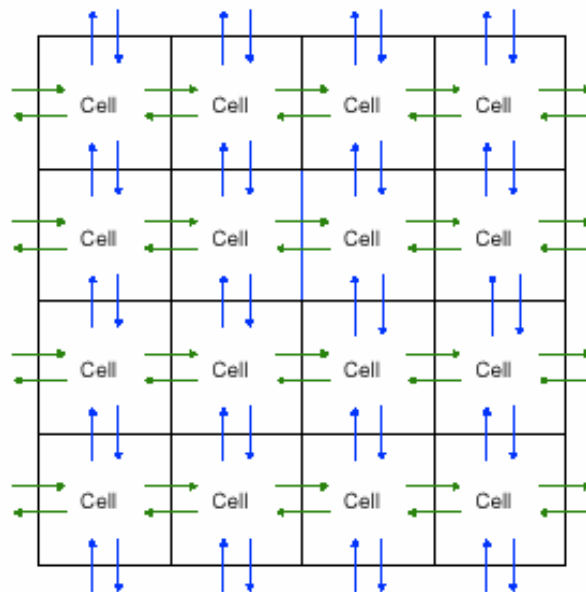
**Figure 2.3 Schematic of the XC6200 Basic Cell**

Figure 2.3 shows the basic cell of the XC6200. The inputs (N, S, E and W) from the neighboring cells and those from the 4 x 4 array cells (N4, S4, E4 and W4) are routed to the function unit. The Multiplexers (MUXs) within the cell are controlled by the configuration memory. The output of the basic cell is routed to its neighbors by the

output routing multiplexers which also provide the redirection function to route the inputs of the function unit to neighbors. With the redirection functions, the basic cell can offer more flexible routing resources.



**Figure 2.4 Schematic of the Function Unit in the XC6200 Basic Cell**



**Figure 2.5 Connections between neighboring Basic Cells**

Figure 2.4 shows the schematic of the function unit. Programming the three MUXs determines the combinational logic operation of this function unit. The RP multiplexer selects the output of the first three MUXs or the sequential logic output from the D-FF and redirects the signal to the D-FF. The CS multiplexer is programmed to pick either

the combinational or sequential logic outputs to be the function unit's output (F). The connection between a Basic Cell and its neighbors is shown in Figure 2.5.

Since most of the delay is caused by the routing wires, the FastLANEs™ is designed to “jump” the signals directly to neighboring 4 x 4 cells (Length 4 FastLANEs™). The Length 4 FastLANEs are shown in Figure 2.6 and the Length 16 FastLANEs™ is shown in Figure 2.7. By using these wires, the propagation delay of a signal transmitted can be smaller than those passed by the Basic Cell's redirection output MUXs. Thus, the FPGA can operate at a higher frequency.

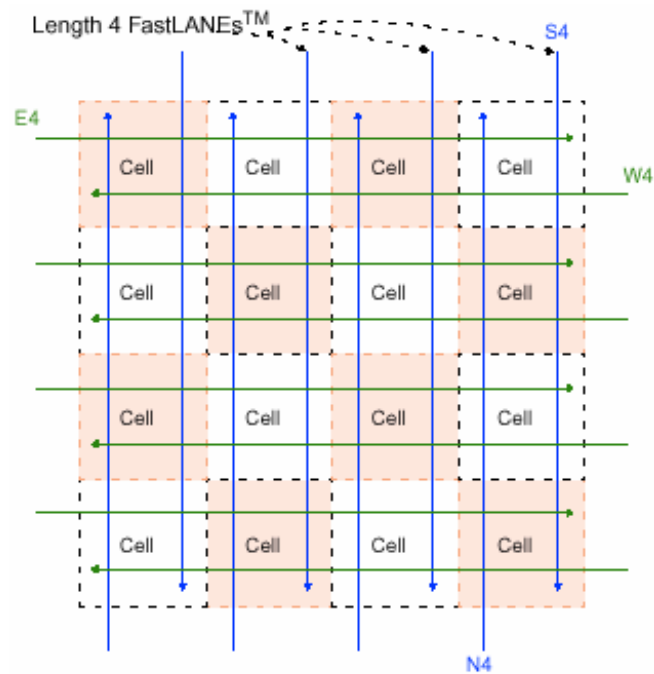


**Figure 2.6 4x4 cell block and Length 4 FastLANEs**

An XC6200 basic cell works in the following way: Each cell receives 2 inputs in each direction. Those inputs are selected by the 8:1 multiplexers, which provide 3 outputs to the function unit as shown in Figure 11. The 3 outputs are sent to the function unit as X1, X2 and X3. After the combinational/sequential (CS) multiplexer chooses one result as a logic result, the logic result is sent to 4 output multiplexers as shown in Figure 2.8. The output multiplexers have two purposes. One is routing the logic result to a neighbor cell. The other purpose is routing a signal from one direction to another

direction.

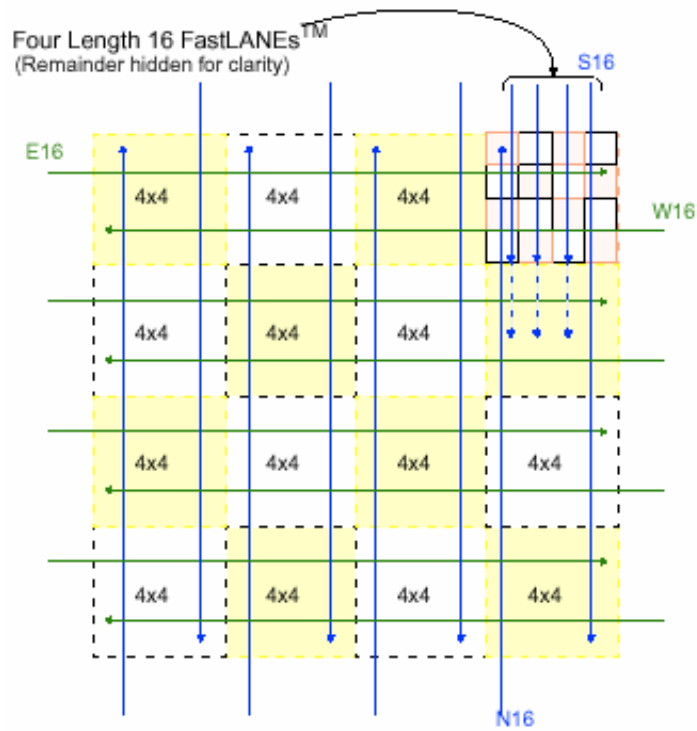


**Figure 2.7 Connections between 4x4 blocks (16x16 block)**

Through the following equation, Table 2.2 shows how the above function unit works to perform different logic functions.

$$Y = X2 \cdot X1 + X3 \cdot \overline{X1}$$

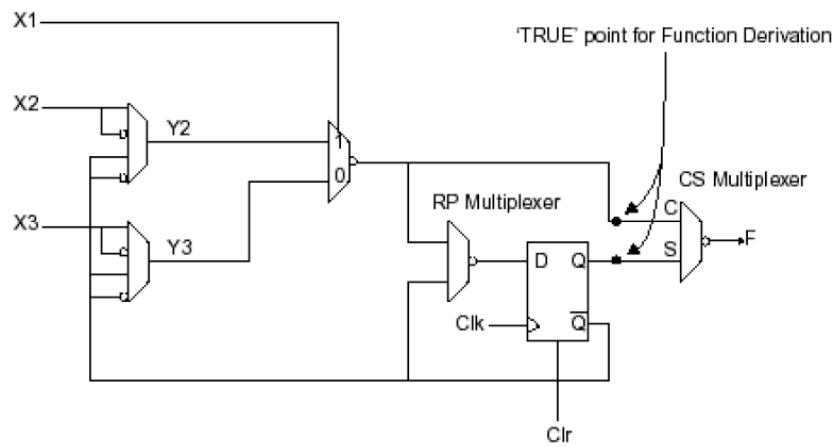


**Figure 2.8 Function Unit of XC6200**

**Table 2.2 Function Derivation Table of the BCII**

<b>Function</b>	<b>X1</b>	<b>X2</b>	<b>X3</b>
<b>0</b>	A	A bar	A
<b>1</b>	A	A	A_bar
<b>BUF</b>	A	A_F	A_F
<b>INV</b>	A_bar	A_bar	A_bar
<b>A and B</b>	A	B	A
<b>A_bar and B</b>	B	A_bar	B
<b>A_bar or B</b>	A_bar	B_bar	A_bar
<b>A nor B</b>	B_bar	A_bar	B_bar
<b>A xor B</b>	A_bar	B	B_bar
<b>A xnor B</b>	A	B	B_bar

## 3 Silicon Germanium (SiGe) Process

### 3.1 SiGe HBT Process Overview

Silicon Germanium (SiGe) Heterojunction Bipolar Transistor (HBT) is the first successful band-gap engineered device.

As the CMOS process develops, the size shrinks thus increasing the number of transistors in integrated circuits. This shrinking process has become a bottleneck in achieving higher performance especially when the oxide thickness becomes small on the order of only a few atomic layers thick. In order to continuously improve a transistor's performance, strained silicon can be used to compensate the increasing carrier mobility.

In 1948, the idea of doping Germanium (Ge) in Silicon (Si) was proposed. A heterostructure device used materials of different bandgaps at the p-n junction, which creates a lowered barrier to hole or electron transport across the barrier, depending on whether the p- or n-type material has the larger bandgap. Silicon crystal has a lattice constant of 5.43, and germanium crystal has a lattice constant of 5.6. The difference in the lattice constants introduces complications when growing silicon germanium on silicon because there is a strain on the SiGe lattice structure as it stretches to conform to the lattice constant of Si crystal. However, stable SiGe crystal can be grown if the layer is thin enough. As the layer thickens, the strain becomes greater and it is less likely that the crystal structure will hold. As mentioned above, SiGe HBTs are formed by growing first a layer of SiGe on Si substrate, while continuously grading the Ge concentration, and then growing another layer of Si on top of the SiGe base. These layers are grown using molecular beam epitaxy (MBE) and chemical vapor deposition (CVD), and more recently, ion implantation has been used to implant Ge content into the base before growing the last layer of Si. Implantation results have been less favorable than the previous two methods, yielding devices more prone to collector-emitter leakage.

After adopting the SiGe hetero-structure, IBM discovered the cost structure and economies of scale were similar to that of Si wafer processing. However, SiGe processing is more complex. In 1996, the first commercial SiGe process was released. This process has revealed that pulling Si crystals apart or straining the Si enables electrons to move through the transistor much faster. With newer generations of SiGe process, its high-frequency performance caught up with the III-V process performances. In this chapter, the details of the SiGe processes are discussed.

The following discussion is mainly based on IBM's SiGe technology since all the chips presented in this document were fabricated through IBM, and all the SiGe documents are accessible to Rensselaer.

Currently IBM has five distinct SiGe HBT BiCMOS technology generations:

- 5HP - 0.5  $\mu\text{m}$ , with a peak fT of 50 GHz
- 6HP - 0.25  $\mu\text{m}$ , with a peak fT of 50 GHz
- 7HP - 0.18  $\mu\text{m}$ , with a peak fT of 120 GHz
- 8HP - 0.12  $\mu\text{m}$ , with a peak fT of 210 GHz
- 9HP - 0.09  $\mu\text{m}$ , with a peak fT of 300 GHz

And more SiGe BiCMOS technologies are presented in Fig. 3.1:

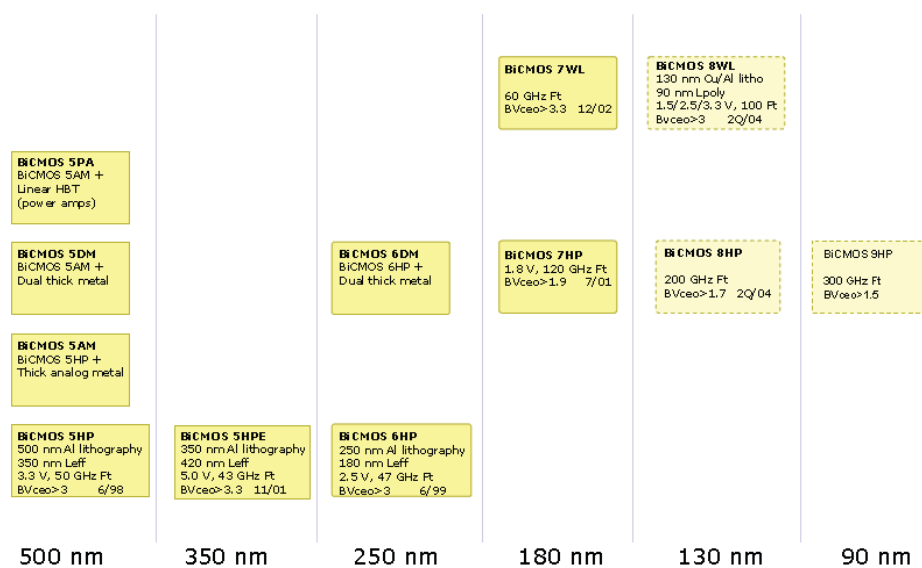


**Fig. 3.1 IBM foundry SiGe BiCMOS technology roadmap**

### 3.2 Performance Advantages

Germanium has a bandgap of 0.661 eV, which is significantly smaller than that of silicon (1.12 eV). In the silicon germanium heterojunction bipolar transistor, germanium is added to the base to narrow its bandgap. In the case of an NPN HBT shown in Figure 13 the bandgap difference allows electrons to more easily overcome the emitter-base junction. The bandgap difference also restricts hole injection across the base-emitter junction.

Using a narrow bandgap material in the base increases the common emitter current gain  $\beta$ , allowing a higher doping level in the base, which in turn lowers base-spreading resistance, an important limiting factor in device frequency determination.

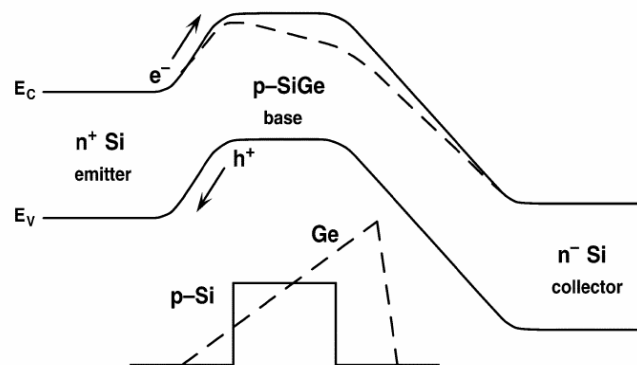


**Figure 3.2 Energy band diagram for Si BJT and graded-base SiGe both biased in forward active mode at low injection.**

### 3.3 Graded Base HBTs

In today's SiGe HBT processes, the Ge content in the base is graded linearly to introduce a built in drift field in the base. This drift field accelerates electrons through the base of the device, reducing the base transit time,  $\tau_b$ . As is evident in the band diagram shown in Figure 1, the graded Ge content is not a necessary precondition for a speed improvement over BJT, but it helps increase the speed of the device even more. However, it is also possible for the positive effects to be negated when the emitter

is more weakly doped by an increased minority charge distribution in the emitter caused by a lowered Ge content at the base-emitter junction.

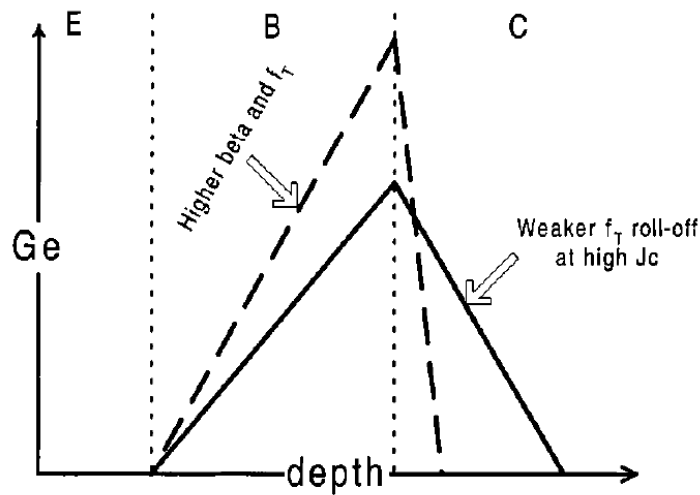


**Figure 3.3 Ge content design trade-off**

As shown in Figure 3.3, the Ge content can be altered in order to achieve different device characteristics. The dashed Ge profile device exhibits higher  $f_T$  and  $\beta$ , and lower noise. However, the solid profile, though lower in  $f_T$ , demonstrates a lower  $f_T$  roll-off at high injection.

### 3.4 IBM SiGe Process

The IBM SiGe BiCMOS process has evolved over several generations, in which the minimum feature size HBTs cutoff frequency reaches 300 GHz (0.09  $\mu\text{m}$  process) and has already been released. Figure 3.4 shows the cutoff frequency of the 0.5, 0.18 and 0.13  $\mu\text{m}$  processes. The cutoff frequency of the IBM SiGe 9HP process approaches 300 GHz. The excellent high frequency performance of the 120 GHz devices has been demonstrated. With its outstanding high frequency characteristics, digital circuits can be created to operate more than 40 GHz. The 0.5  $\mu\text{m}$  (43 GHz) process was the one used to fabricate the first generation Configurable Logic Block (CLB). The 120GHz/0.18 $\mu\text{m}$  (7HP) process was used for most of the subsequent designs.

Figure 3.4 depicts the collector current in logarithmic scale versus the operating speed ( $f_T$ ) of the device. If the  $I_C$  is decreased by half, the  $f_T$  of the HBT decreases by a much smaller percentage. For example, in the IBM SiGe 0.18  $\mu\text{m}$  generation, the collector current is 1.1 mA at its maximum frequency (124 GHz). Half of the current yields a cutoff frequency of 80 GHz which is still fast enough for the FPGA configurable cell. This advantage can be used to create a circuit with lower power consumption while experiencing little performance degradation.

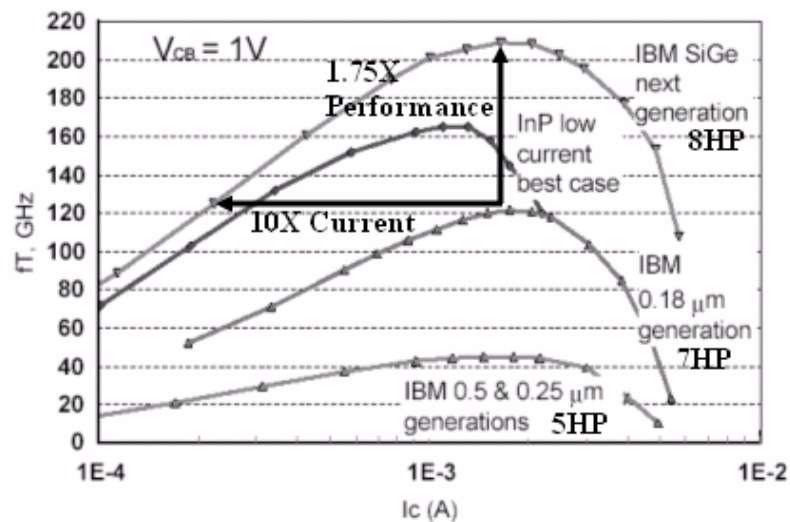


Figure 3.4 Cutoff frequencies of several SiGe Technologies

Fig. 3.5 is the plot of  $f_T$  for 7HP technologies, using which the two big scale FPGA chip was fabricated.

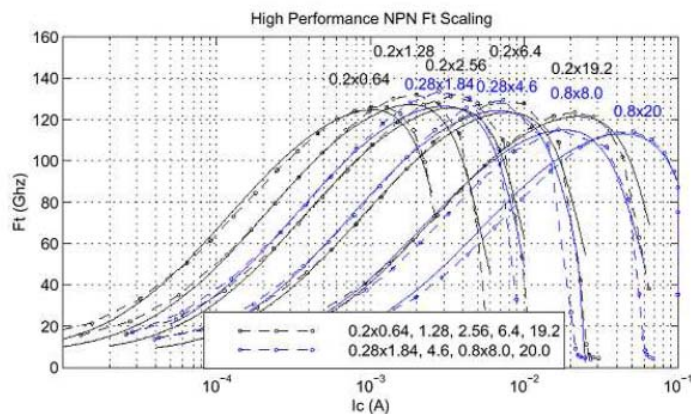


Figure 3.5  $f_T$  vs.  $I_C$  curve for IBM SiGe 7HP technology

Fundamentally, the strained SiGe layer reduces the band gap of the base, emitter charge storage and base transit time while increasing the emitter injection efficiency. Therefore, compared to the Si-BJT, the graded Ge profile in the SiGe HBT increases  $f_T$  without degrading breakdown voltage ( $BV_{CEO}$ ). Graded SiGe base transistors have the added advantage of higher Early Voltage ( $V_A$ ) along with higher  $f_T$  and  $BV_{CEO}$ . The drift field from the graded Ge profile provides additional driving force for carrier transport across the neutral base. An additional advantage of SiGe HBTs is that the base is formed by epitaxy. The base doping can be made higher. This limits the depletion length into the base at the base-collector junction, decreasing the modulation of the bandwidth. Thus, the Early voltage is not degraded by high collector doping for a graded SiGe base compared to a homojunction device. The HBT characteristics of a 0.5  $\mu\text{m}$  (5HP), a 0.25  $\mu\text{m}$  and a 0.18  $\mu\text{m}$  generations are summarized in Table 3.1. It is found that the higher frequency operation of an HBT implies lower breakdown voltage.

**Table 1.1 HBT comparison for 0.5  $\mu\text{m}$ , 0.25  $\mu\text{m}$ , and 0.18  $\mu\text{m}$  generations.**

Parameter	0.5 $\mu\text{m}$	0.25 $\mu\text{m}$	0.18 $\mu\text{m}$
$A_E$ ( $\mu\text{m}^2$ )	0.5 x 0.25	0.44 x 3	0.18 x 0.82
$\beta$	100	100	200
$V_A$ (V)	65	75	120
$BV_{CEO}$ (V)	3.35	3.35	2.5
$BV_{CBO}$ (V)	10.5	10.5	7.5
$R_B$ ( $\Omega$ )	124	114	60
$R_E$ ( $\Omega$ )	16	X	X
$f_T$ (GHz)	47	47	90
$f_{MAX}$ (GHz)	65	65	90

Higher  $f_T$  s are being required by circuit designers to satisfy the ever-expanding demand for bandwidth. A conservative rule of thumb is that, for digital parts, the technology must be capable of supporting flip-flops that run at twice the bit rate. For example, the synchronous data transmission on optical media provides some of the highest speed requirements. Currently one of the highest network standards is OC-192 or

approximately 10 Gbps networks. Since the best flip-flop performance possible is approximately one half  $f_T$ , so that an  $f_T$  of four times the bit rate, or 160 GHz for a 40 Gbps SONET applications can be obtained. While designing a circuit, a designer should consider  $f_T$ ,  $f_{MAX}$ , and other characteristics.

### 3.5 Current Mode Logic (CML)

Different digital circuit families are available for use with bipolar devices. Some of the well known families are Resistor Transistor Logic (RTL), Transistor Transistor Logic (TTL), Integrated Injection Logic (IIL), Emitter Coupled Logic (ECL), and Current Mode Logic (CML). The switching speed of the devices and the circuit driving requirements affect the choice of the digital circuit family.

In a bipolar device the amount of charge and the speed of the displacement of this charge in the base region determine the conduction of current from the collector to the emitter. In order to saturate the device a large amount of charge needs to be accumulated in the base of the device. To achieve higher switching speeds saturation of the device has to be avoided. The ECL and CML families operate the devices in the forward active and cut-off regions so that the amount of charge required is significantly less than the other circuit families, therefore these families provide higher switching speeds.

CML is the second generation of Emitter Coupled Logic (ECL). Like ECL, it is a differential logic design methodology that focuses on steering currents instead of switching them. It has many similarities to ECL designs, such as preventing the transistor from saturating and wide use of emitter coupled differential pairs. The benefits of utilizing the fully differential logic are: relative immunity to noise (especially power and ground noises) and simplification of logic. Through the use of differential signals an inversion can be realized by simply switching wire polarity without incurring any delay.

Beside the advantages that stem from the differential pair configuration, CML also has the advantage of not requiring emitter followers at the gate outputs and it can be

biased at lower current levels without significantly degrading its speed. Overall, less power is consumed with CML than ECL since CML normally runs at the currents around 0.1 ~ 1 mA compared to ECL's 1 ~ 10 mA. The performance of CML is compared to ECL and shown in Figure 3.6. From this figure, it can be found that when the switching frequency is set to 40 GHz, the power consumption of the CML is about half of ECL.

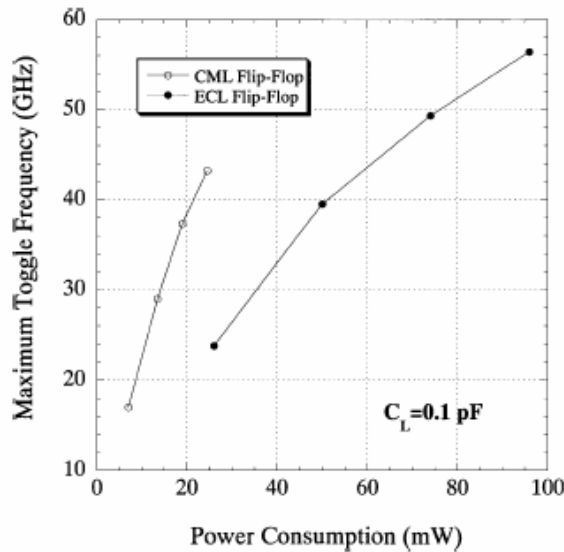


**Figure 3.6 Max. Switching frequency versus power consumption of CML and ECL logic**

Figure 3.7 shows a CML buffer. A reference current ( $I_{ref}$ ) is provided at the bottom of the current tree. By properly steering the current flow through the switching transistors ( $Q_1$  and  $Q_{1b}$ ) and the collector resistors; the desired output voltage is achieved.  $I_{C1}$  and  $I_{C1b}$  can be calculated by Eq-3.1 to Eq-3.4 listed in Table 3.2. The collector current of a forward bias device as a function of  $V_{BE}$  is approximated as Eq-3.1. Using this equation, it is possible to divide the collector current of the first device by that of the second in order to understand the ratio of the collector currents in a differential emitter couple pair by Eq-3.2. If the current is flowing through the emitter couple pair to the current switch on the bottom, it can be expressed by Eq-3.3. From Eq-3.2 and Eq-3.3,  $I_{C1}$  and  $I_{C1b}$  can be described by Eq-3.4 and plotted in Figure 12 for different  $\beta$  (the ratio of the base current to collector current). In this equation, when  $V_{id}$  equals zero, the current is evenly divided between  $I_{C1}$  and  $I_{C1b}$ . Since there is always constant current flowing in

the CML, the static power consumption (Eq-3.5) of the CML is the total power consumption.

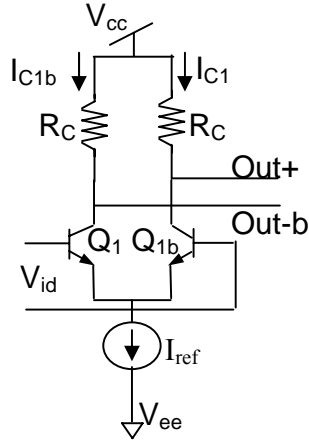


**Figure 3.7 A conventional CML Buffer**

**Table 3.2 Equations of the CML buffer**

$I_C = I_S \exp \left( \frac{qV_{BE}}{mkT} \right)$	Eq-3.1
$\frac{I_{C1}}{I_{C1b}} = \exp \left[ \frac{qV_{id}}{mkT} \right]$	Eq-3.2
$I_{CS} = \frac{\beta + 1}{\beta} (I_{C1} + I_{C1b})$	Eq-3.3
$I_{C1} = \frac{\beta}{\beta + 1} \frac{I_{ref}}{\left[ \exp \left( \frac{qV_{id}}{mkT} \right) + 1 \right]}$	Eq-3.4
$Static\_Power = (V_{CC} - V_{EE}) \times I_{REF}$	Eq-3.5
$ V_{EE-min}  = 2V_{BE} + V_{REF}$	Eq-3.6
for the two input levels situation	

The value of the input differential voltage that fully switches the current to one side is about 200 mV. Therefore, most CML circuits operate at an input and output voltage differential larger than 200 mV. The CML used in this design has three different voltage levels to provide proper input signals. The ranges of those levels are Level 1: 0 ~ -0.25 V, Level 2: -0.95 V ~ -1.2 V and Level 3: -1.9 V ~ -2.15 V.

The equation for calculating the voltage of input levels is listed as Eq. 3.5. Fig. 3.9 shows the CML D-FF which has the D (D-b) connecting to level 1 inputs and the CLK (CLK-b) connecting to the level 2 inputs. The performance and power consumption of CML logic family are summarized in Table 3.3. Based on this table, one can observe that the propagation delay of the CML family is much smaller than CMOS circuits. Figure 3.10 shows the propagation delay of a CML buffer with the emitter size of 0.2 x 0.64  $\mu\text{m}^2$  versus the biasing current ( $I_c$  in mA). It can be observed when the bias current

is increased, the propagation delay is reduced. When the biasing current reaches to 0.5~0.6 mA, the curve reaches the saturation region and the propagation delay does not significantly change if the reference current increases. The curve can be approximated

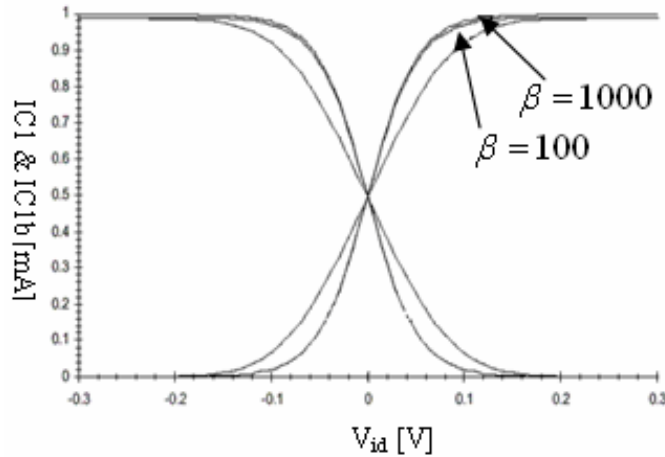


**Figure 3.8 Transfer characteristics of the CML buffer at different values of  $\beta$**

**Table 3.3 Performance of the SiGe CML**

Circuit type	CML buffer	CML AND, OR, XOR	CML MUX	Configurable Logic Block
Propagation delay	17 ps	22 ps ~ 25 ps	23 ps ~ 26 ps	100 ps
Current used	0.7 mA	0.8 mA	0.8 mA	2.4 mA
Power used	3.15 mW	3.6 mW	3.6 mW	10.8 mW
All the above results are based on IBM SiGe 5HP process				

with piecewise lines with a slope of -25 ps/mA in the first section and a slope of -4 ps/mA in the second section.

From the above paragraphs, in summary, the speed of a device can be traded off for reduced power consumption in a logic tree. The biasing current is set to 1 mA in most cases described in this thesis. Those results also show that if the current is reduced by

half, for example to 0.5 mA, the power consumption can be reduced by half with the propagation delay increased by 2 ps. This design idea imitates the Power Saving Mode CML circuit described later.

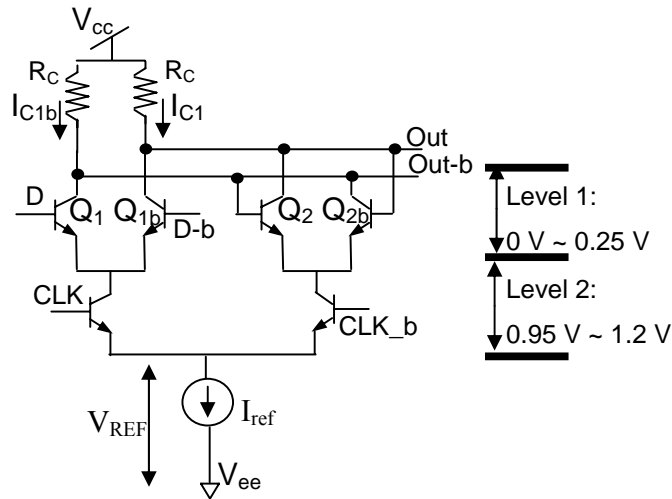


**Figure 3.9 CML D-latch configuration with two input levels**

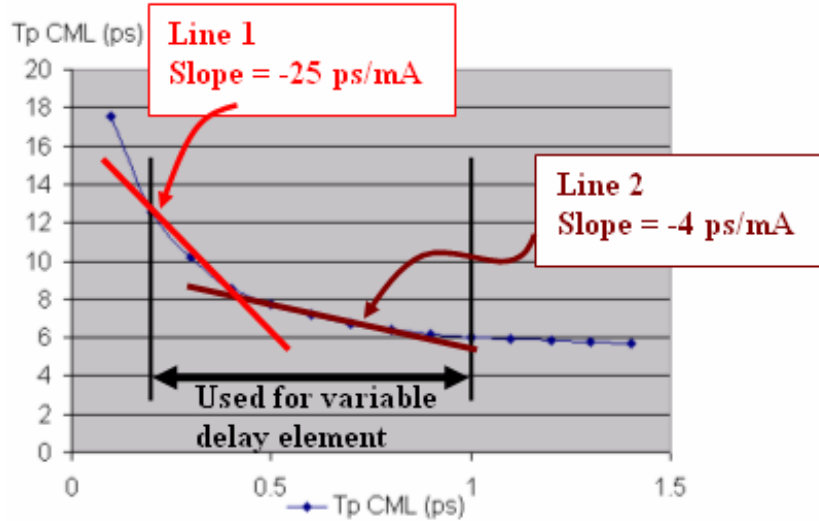


**Figure 3.10 Propagation delay of the CML buffer**

**with the emitter size of 0.2 x 0.64  $\mu\text{m}$ .**

### 3.6 Difficulties of designing a CML high speed FPGA

The power consumption of the first SiGe CLB was about 10.8 mW, which is larger than its CMOS competitors. To realize a large scale CML FPGA, some power-saving strategies have to be applied. Four methods are provided to solve the power consumption problem.

1. The first method is to reduce the reference current in the tree to decrease the static power consumption by sacrificing the speed of the transistors. From Figure 3.5, the cutoff frequency (120 GHz) of the 0.18  $\mu\text{m}$  process has a maximum value when reference current equals to 1.1 mA. If the current is reduced by half, 0.5 mA, the cutoff frequency of the SiGe HBT only drops to 80 GHz which is a 35% reduction. This implies that by compromising bandwidth of an HBT, the current can be reduced to lower the power consumption of CML circuits.

2. Second, the power supply voltage can be reduced to further decrease the static power consumption. Based on Eq. 3.5 in Table 3.2, if the power supply can be reduced by half, the total power consumption can be decreased by half.

3. Third, by combining the logic in a circuit, the number of the CML trees can also be decreased too.

4. Lastly, turning off unused circuits and combining some logic blocks in the Basic Cell can further lower the power consumption.

The first strategy leads to future larger scale FPGAs. The second, third and last strategies lead to a modified CLB design. Both designs improvements are described in the following chapters.

## 4 Large Scale (16 x16 BC array) SiGe FPGA design

In this chapter, a 16 x 16 BC array SiGe FPGA with 2.8 V power is presented. The detailed schematic, layout and design considerations are described. Figure 4.1 shows the block diagram of the SiGe 16 x 16 BC array FPGA. It is designed to perform 4-bit logic operations. Four sub-blocks are included; they are the FPGA core, input multiplexer block, output selection block and oscillator.

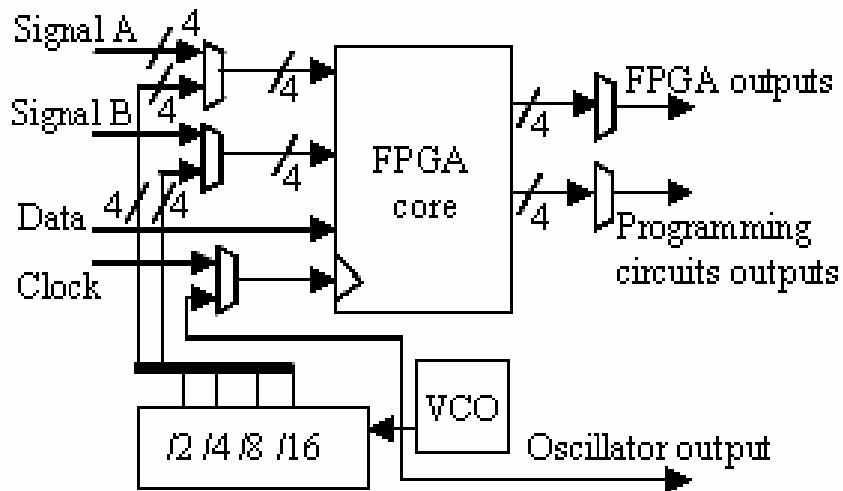


**Figure 4.1 Block diagram of the 16 x 16 array FPGA.**

The input multiplexer block has two 4-bit MUXs used to multiplex the selected external signals (Signal A and B) and the test signals generated from the frequency divider. The outputs of four BC blocks can be selected as the FPGA output after the selection of the output MUX. The detail functions of the blocks in Figure 4.1 are explained in the following paragraphs.

### 4.1 The XC 6200 Basic Cell

A reduction in the number of CML trees per Basic Cell results in lower power consumption for the entire design. Therefore, one of the goals is to simplify logic gates of the Basic Cell in the Xilinx 6200 FPGA. The Basic Cell block diagram shown in Figure 4.2 consists of input/output routing blocks and a Function Unit (FU). The input

routing block is composed of three 8:1 multiplexers (MUXs) to route the outputs from the surrounding Basic Cells (coming from N, S, E, W) into the Function Unit. The RP MUX routes the combinational signal and the sequential signals into the D-FF. The CS MUX, which selects combinational or sequential logic, routes the chosen signals to the output routing block, consisting of four 4:1 MUXs. The output routing block then routes the signals to the neighboring Basic Cells. The Basic Cell schematic is redrawn and shown in Figure 4.1.

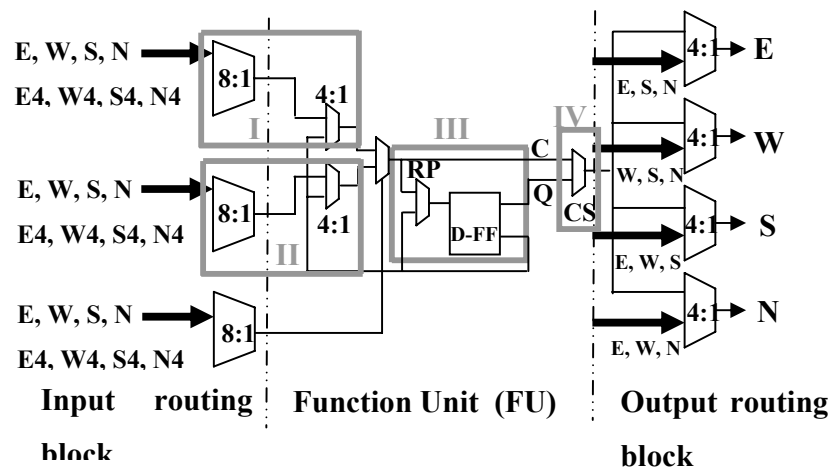
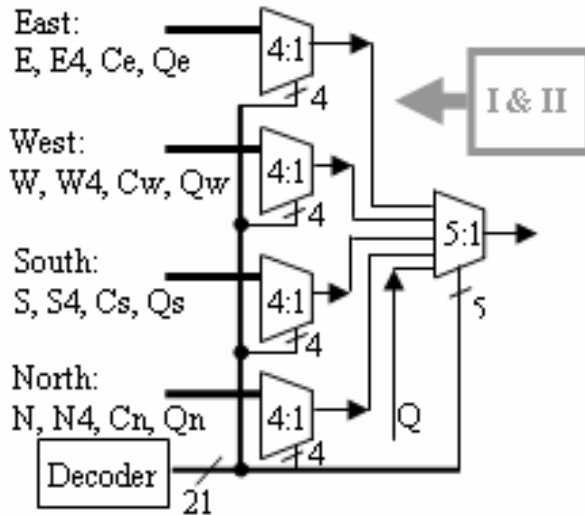


Figure 4.2 XC6200 Basic Cell.

#### 4.1.1. Input routing block

The input routing block combines the logic functions of the 8:1 MUX and 4:1 MUX, shown in the gray blocks I and II of Figure 4.1 to a new MUX. In Figure 4.2, the new input routing block separates the signals by their incoming directions. All the input signals coming from the same direction (N, S, E and W) are connected to the same 4:1 MUX. For example, all signals originating east of a Basic Cell are connected to one 4:1 MUX. The 8:1 MUX in the original design is broken down into four 4:1 MUXs from all directions, and the four 4:1 MUX outputs are combined with the output of the D-FF in a second level 5:1 MUX. Advantages of this combination are reduction in circuit complexity and propagation delay while maintaining full compatibility with the original 6200 configuration bit streams.

The MUXs used in the input routing block have been redesigned as well. The general form of the new design circuit is shown in Figure 4.3. The differential input pair



**Figure 4.3 Redesigned input routing block. Label Ce indicates combinational logic (C) from the east.**

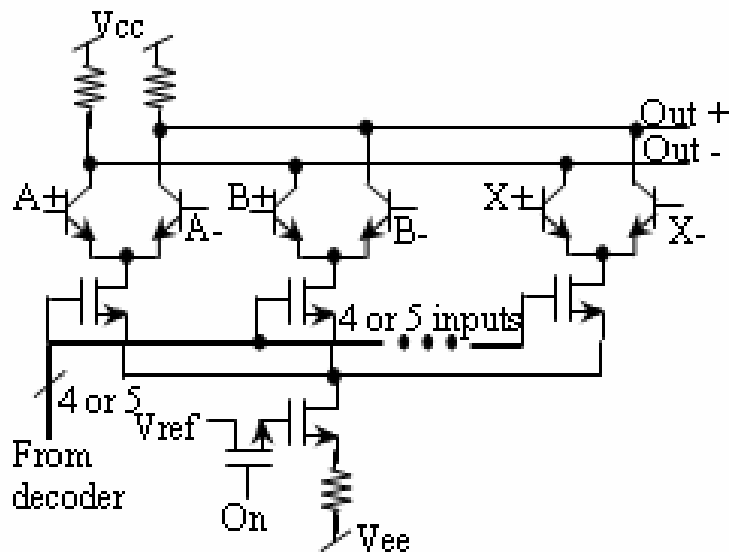


**Figure 4.4 General form of the new MUX design. The new input routing stage has 4:1 and 5:1 MUXs and the new output routing stage has 4:1 MUXs.**

of transistors is connected to the drain of an NMOS switch. Only one pair can be selected in a MUX, so with the use of a decoder the desired differential input pair can be

selected and the remaining pairs turned off to save power. The output MUXs have the same configuration.

#### 4.1.2. Function Unit (FU) in the new Basic Cell

In block III of Figure 4.2, the RP MUX was merged into the D-FF, thus further reducing the number of CML trees. Since another input level for the RP selection control is inserted into the D-FF, the CML tree will be taller. Reducing the height so that a smaller power supply can be used is crucial. The schematic of the new D-Flip Flop after merging with the RP MUX is shown in Figure 4.4 for Latch 1 and Figure 4.5 for Latch 2.

The main concepts of designing the new MUX focus on how to properly steer the current into independent current trees. By adding a switch to the Vref transistor in the CML tree, the entire tree can be turned off. In Figure 4.5 showing the Latch 1 design of the new D-FF, if combinational data C (C+ / C-) is the desired input, the On-2 can be disabled and On-1 can be turned on. To select sequential data Q (Q+ / Q-), the On-1 should be turned off and On-2 be turned on. With the use of the switches, the functions of the RP MUX can be completely merged into the first latch. In Latch 2, there are two current trees. However, only one current tree will be turned on at any given time, similar to Latch 1. One tree is for the D-latch logic and the other is for “CLEAR” (CLR) to directly pull down the output to the lowest voltage in the circuits. With this design, there can be two input voltage levels with the power supply voltage equals to 2.5 V.

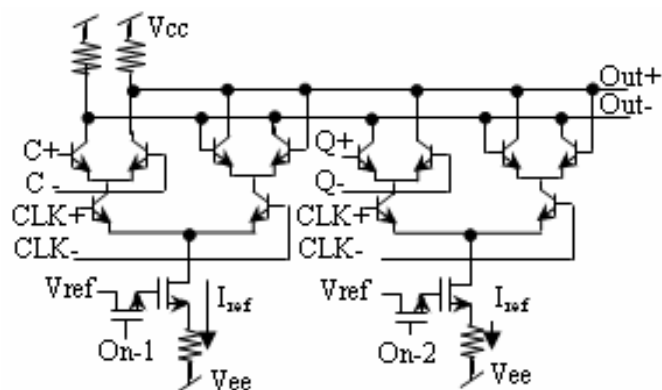
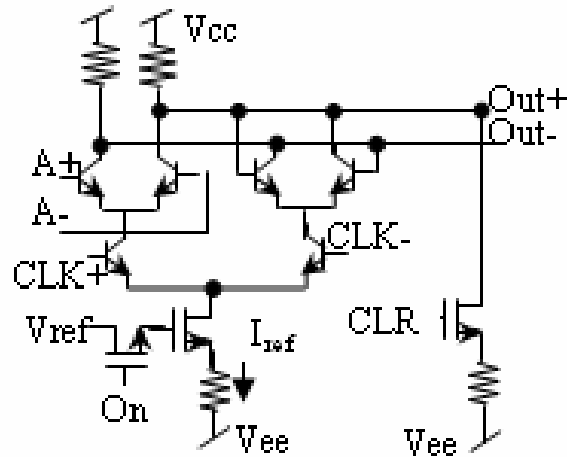
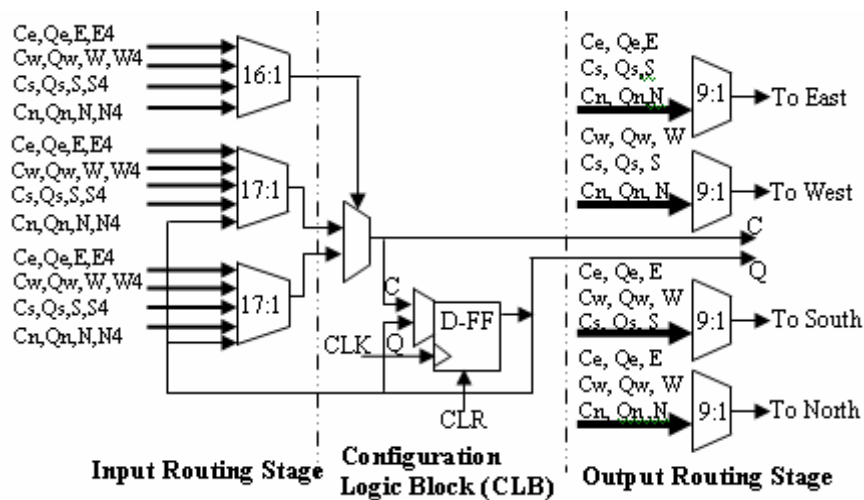


Figure 4.5 Latch 1 in the new D-FF design.



**Figure 4.6 Latch 2 in the new D-FF design.**

The CS MUX, shown in block IV of Figure 4.2, is used for selecting either combinational logic (C+, C-) or sequential logic in the original design. With the new input stage, this job is now done at the next Basic Cell's input routing stage, so the CS MUX can be removed from the Function Unit in the new Basic Cell to reduce the total gate delay. The new Basic Cell structure is shown in Figure 4.7. It is created by simplifying and combining the four blocks (I, II, III and IV) drawn in Figure 4.2. The overall functions of the Basic Cell remain the same as in the original design to keep the same bit stream and use the existing software (Xilinx 6200) to program them. After



**Figure 4.7 Schematic of the BCII.**

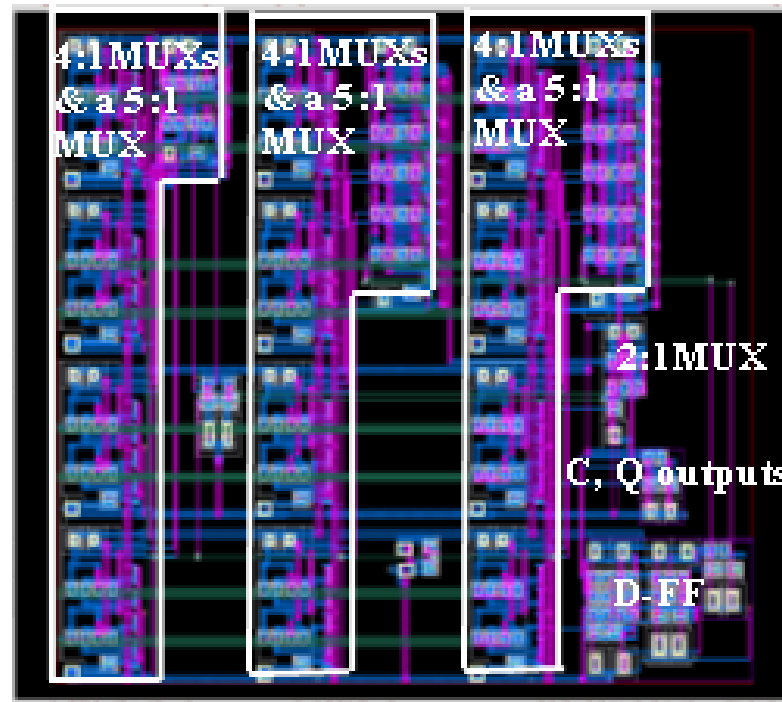


**Figure 4.8 Layout of the Basic Cell**

developing the new Basic Cell, the total number of current sources has been reduced from 30 (14 CML trees, 8 pairs of the emitter followers) to 21 (13 CML trees, 4 pairs of emitter followers) and the propagation delay has been reduced as well. The layout of the new Basic Cell is shown in Figure 4.8 with the dimension of 230 x 170  $\mu\text{m}^2$ .

#### **4.1.3. Dynamic shut down of unused circuits**

The NMOS switches in every MUX and D-FF can be used to disable the unused circuits. Thus, it can be used to shut down unused current trees in the programmed Basic Cell to reduce power consumption. In the worst case (Basic Cell maximum usage case), there will be no circuits that can be turned off.

In Case I, there is a combinational or sequential function enabled and no redirected signals. The signals come in from the input routing block and passed to the Function Unit (FU). In this case, there are 10 or 12 current trees turned on. In the second case

(Case II), the Basic Cell is programmed to perform sequential logic and the input signals are also redirected to the output routing block.

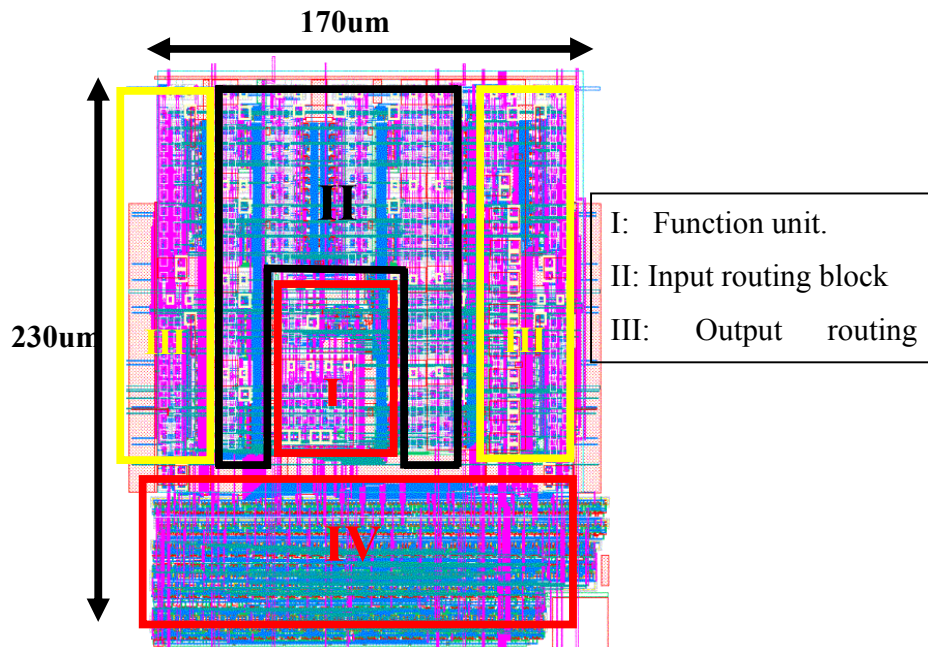


Figure 4.9 Layout of the new Basic Cell

Table 4.1 Dynamic Routing Power Usage

Case I. Only combinational logic or sequential logic is used.

Case II. Sequential logic and redirection function are used.

Case III. Only redirection function is used.

Design		Tree #	Power Usage
BC Maximum Usage		21	100%
Case I (Comb./ Sequential Logic)		10 / 12	47.6% / 57.1%
Case II	Sequential, One Redir.	15	71.4%
	Sequential, Two Redir.	18	85.7%
	Sequential, Three Redir	21	100%
Case III		3 tree / dir	14.2% / dir

Based on how many signals are redirected, the numbers of the current trees enabled are: 15 for one redirected signal, 18 for two redirected signals and 21 for three redirected signals. The above results are summarized in Table 4.1.

## 4.2 Voltage Controlled Oscillator (VCO) in SiGe FPGA

In the 16 x 16 BC array FPGA, its clock is generated from a Voltage Control Oscillator (VCO) which is a four-stage ring oscillator shown in Figure 4.10 (a). A modified Gilbert mixer is used as its building block. This VCO can linearly interpolate the signals received from the previous two stages. Each stage mixes the signals from previous stage and the stage preceding that one. For example, the output signals of the buffer B depend on the signals from A and D buffers. These signals are weighted by the control signals of the mixer and summed by the pull-up resistors. The minimum operating frequency is defined by the case when the leap signal is ignore, which is shown in Figure 4.10 (b).

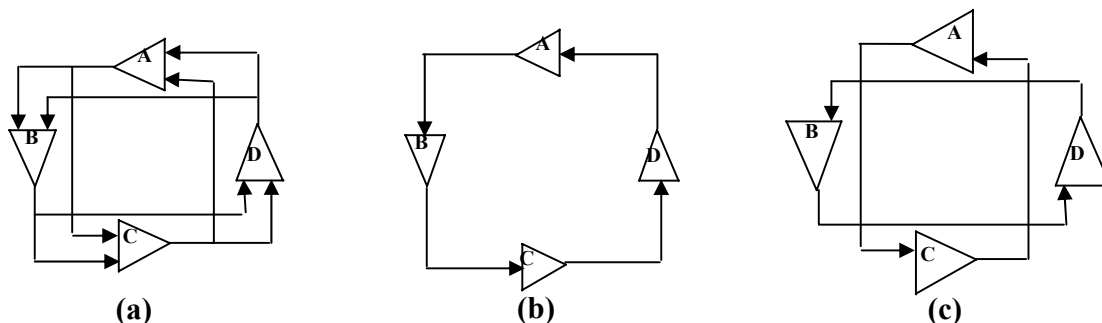


**Figure 4.10 the VCO's architecture (a) Feed Forward VCO block diagram. (b) The VCO running in the four stage configuration with the control voltage set to a minimum value. (c) The VCO in the two stage configuration at the maximum control voltage.**

The VCO's maximum frequency can be achieved by ignoring the previous stage signals. Thus, the oscillator runs as a two stage ring oscillator (Figure 4.10 (c)), which has a higher frequency than 4-stage case (Figure 4.10 (b)). Figure 4.11 shows the schematic of the VCO multiplexer. It linearly interpolates the signal from the previous

stage (A20, A21) and the buffer previous to that stage (B20, B21) through the control voltage (C30, C31). Resistor Rb limits the operating range of the VCO, Re adjusts the control voltage range and capacitor Cc defines the operating range. In the 16 x 16 FPGA, the VCO was designed to run in the range between 7 and 13 GHz with the center frequency at 10 GHz. Figure 4.12 shows the layout of the VCO which is symmetrical to minimize unbalanced parasitic effects caused by different lengths of wires.

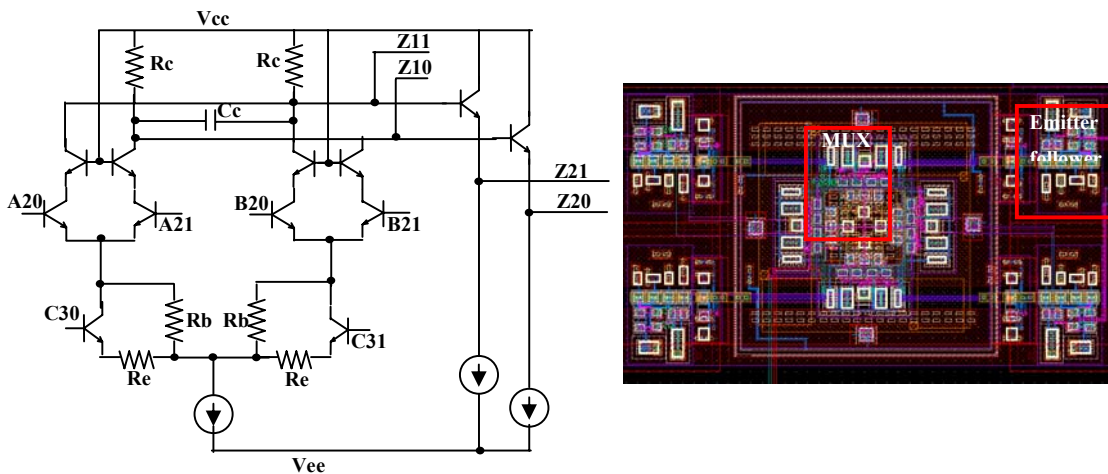


Figure 4.11 Schematic of the VCO buffer. Figure 4.12 Layout of the VCO buffer.

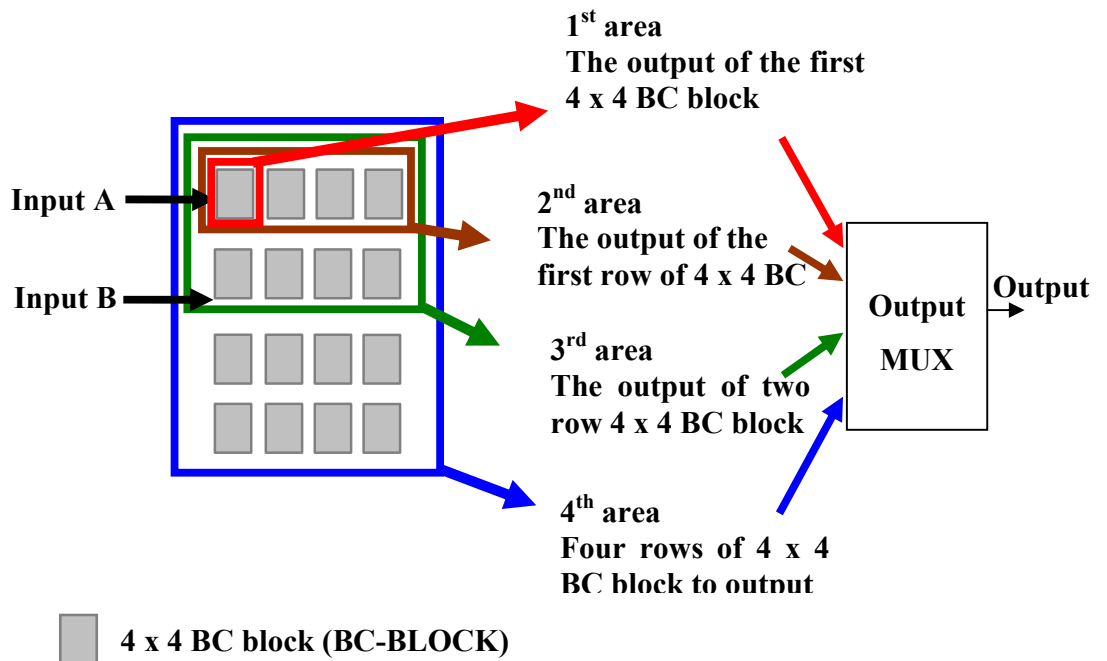


Figure 4.13 Block diagram of the input/output blocks and the FPGA core.

### 4.3 Input multiplexer block, output selection blocks and FPGA core

The data flow of the FPGA is shown in Figure 4.13. The FPGA core, located in the center, is constructed of five 4 x 4 BC arrays (BC-BLOCKS). Depending on the number of BCs that an application needs, one of four portions of the BC array is activated. The first portion is the first BC-BLOCK, the second portion is the first row of BC-BLOCKS, the third portion is the first two rows of BC-BLOCKS and the last is the whole BC array. The two input 4-bit signals (A and B) are routed to the first and second row of the BC BLOCKS. Two MUX selection signals decide whether the internal or the external signals are routed to the core. All outputs must be routed to an output MUX which connects to the external pads.

### 4.4 Programming scheme in the Basic Cell and FPGA

To test this FPGA, it is very important to have a robust and simple programming structure. There are several ways to program it. Using shift registers to transport data into memory is one of the simpler methods. The advantages of using a shift register structure are ease of scaling up, reduced timing constrains, and a relatively simplified structure. The drawbacks are its circuit layout occupies more area than other memory structures (DRAM) and the time to program all the memory cells is longer. In this FPGA, we don't need to care about the speed to program memory cells. Therefore, the shift register structure was picked to program this SiGe FPGA chip.

#### 4.4.1 Programming structure used in Basic Cell

The programming structure of the Basic Cell includes two parts. One is the shift register and the other is the memory bank. Its schematic is shown in Figure 4.14. Since this part doesn't have to run at very high speed, the timing constrain of the clock is not as critical as the FPGA core, however the signal strength of the clock and data must be guaranteed. Therefore, repeaters have been placed to insure the clock reaches its logic

high level. Data is shifted to the shift register. After n clock cycles, the data is shifted to the desired position and an enable signal is generated to write the data to memory.

Since the shift register has expandable capability, it can be serially connected to the other Basic Cells. Its structure and function have been described in the previous paragraph. Figure 4.15 shows the layout of 42 SRAM cells. It is composed of two rows of 21 SRAM cells. Figure 4.16 shows the layout of the 42-bit shift register. It is composed by 6 D-FFs in each row and the output of the previous row serially connects to the following row's input.

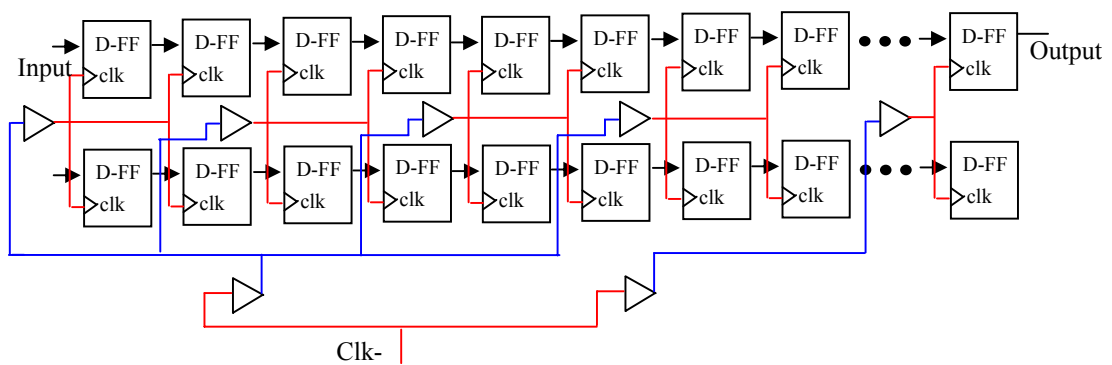


**Figure 4.14 Schematic of the programming scheme with clock distribution.**



**Figure 4.15 Layout of 42 SRAM cells**

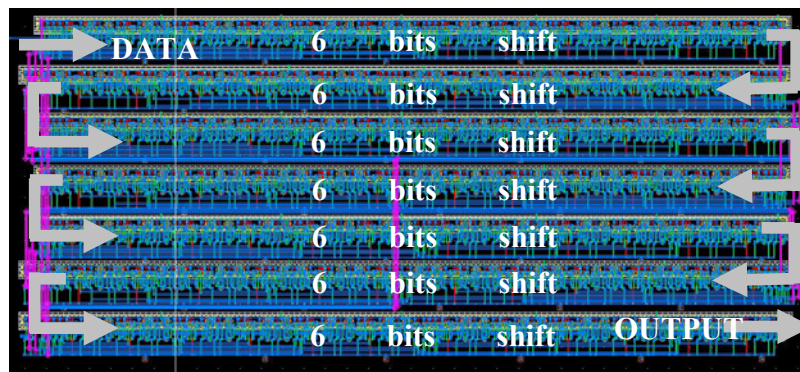


**Figure 4.16 Layout of 42 bits shift register.**

The above circuits were simulated with a 500 MHz clock at a temperature of 50°C. Figure 4.17 shows the simulation result of the 42-bit memory circuit. When WR-EN is zero, the outputs of the 42 memory bits are all “one”. While the WR-EN changes to high, the data is latched into the memory and programs the Basic Cell. Figure 4.18 shows the simulation of the shift registers. The first four outputs are monitored. In those outputs, the data is propagating from one flip flop to the next one.

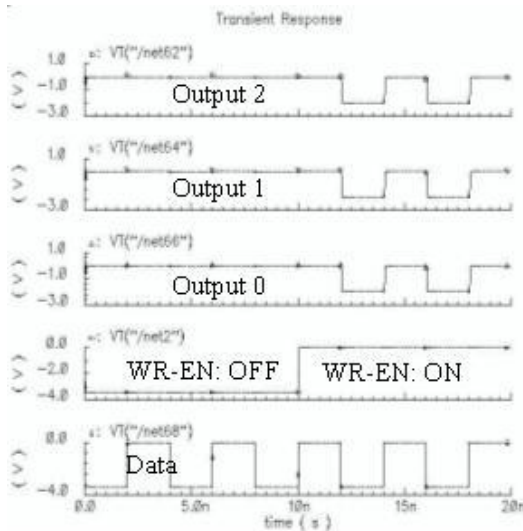


**Figure 4.17 Simulation of the 42-bit memory.**

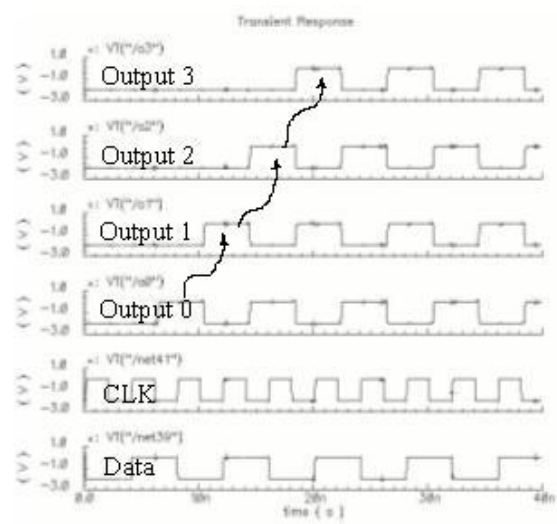


**Figure 4.18 Simulation result of the shift register output with input data period of 800 ps.**

#### 4.4.2 Programming circuit in the 16 x 16 FPGA

There are two methods to program the configuration bit stream into an FPGA. The first method is to use the DRAM structure. It has to deal with read (write) timing issues which make the memory systems much more complicated to design. Another method is to use the shift register structure to reduce the complexity of the memory structure and shift the data stream to the corresponding memory positions. Figure 81 shows the connection of a row of Basic Cell in the 16 x 16 FPGA. A long chain of shift registers can be formed to increase the flexibility of the hardware scale. Data can be passed to every Basic Cell to program desired functions. Then the data path is connected to the input of next row of Basic Cell.

By connecting all shift registers in the 16 x 16 FPGA, the FPGA's personality can be programmed. Figure 4.19 shows the programming scheme of the SiGe FPGA. The center-to-center spacing of the BC is about 170 $\mu$ m. CMOS data repeaters (CMOS buffer)

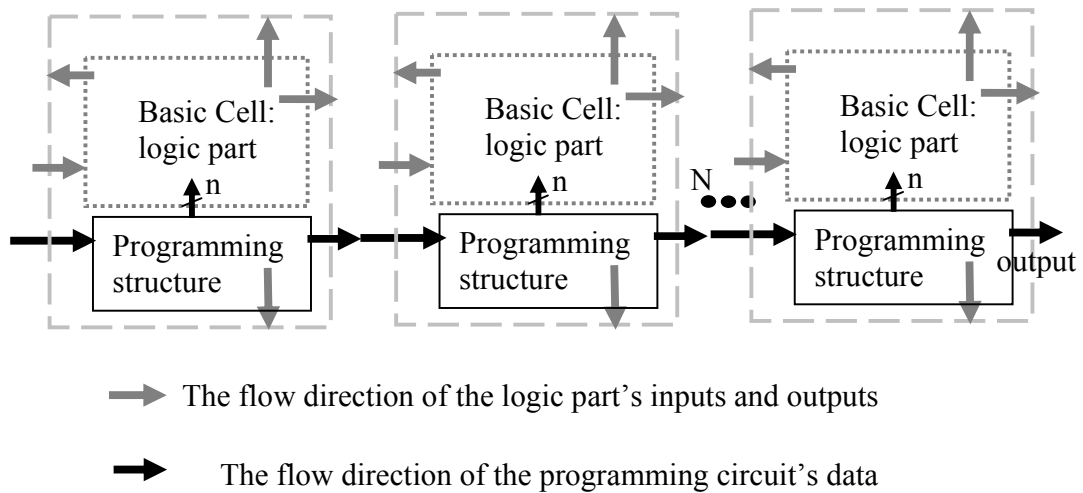


**Figure 4.19 Block diagram of an array of basic cells with programming circuits connected**

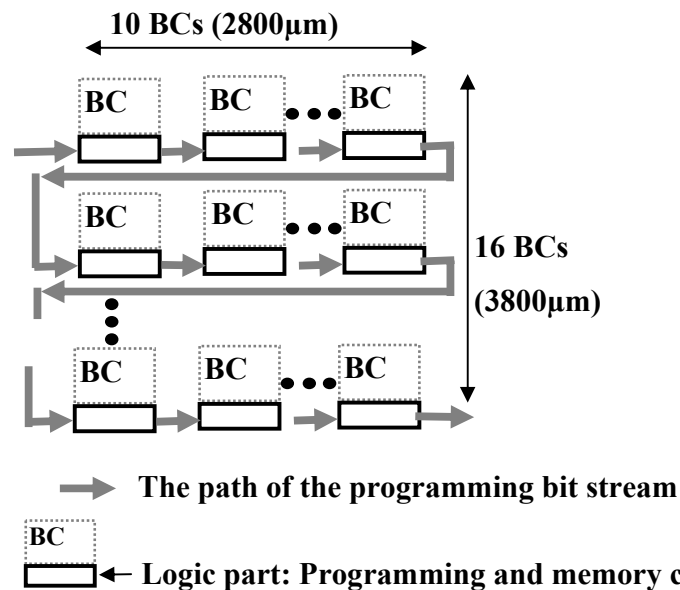


**Figure 4.20 Programming and memory circuits in the SiGe FPGA**

are inserted to boost up signal strength. To make sure that the configuration bits of the 20 x 20 SiGe FPGA correctly arrive at their positions, the data in each row of BC can be routed outside of the chip and compared with the input data.

## 4.5 Power Rails design

In Figure 4.21 (a) and (b), the black and gray wires show the  $V_{cc}$  (0 V) and  $V_{ee}$  (-2.8 V) power rails. Since the voltage is gradually lost along the wires due to parasitic elements, it is very important to design power rails that have no large voltage drop between the ends of rails. Table 4.2 shows some important parameters of the SiGe process. In order to get a good estimation of the power rail width, some assumptions must be made;

1. The length of the Basic Cell is  $170\ \mu\text{m}$  with an additional  $5\ \mu\text{m}$  spacing to the next Basic Cell. ( $L = 175\ \mu\text{m}$ )
2. The thickness and width of the AM metal are both  $4\ \mu\text{m}$ .
3. The current that each BC consumes is  $1\ \text{mA}$  (in the 8HP IBM model manual,  $f_{T\text{max}}$  can be achieved at  $I_c = 1\ \text{mA}$ ).
4. All the current trees in the Basic Cell are on (22 current trees;  $22\ \text{mA}$ ).
5. The voltage at the end of the power line is less than  $2.79\ \text{V}$ . The allowable voltage droop is 1% since the input power is  $2.8\ \text{V}$ .

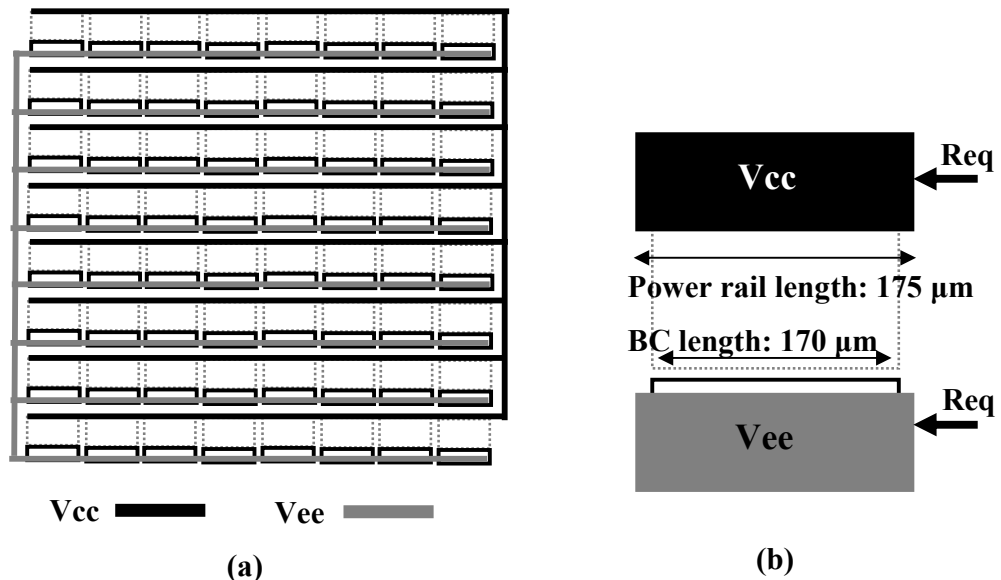


Figure 4.21 (a) Power rail in the FPGA core. (b) Power rail in each BC.

**Table 4.2 Characteristics of the metal layers of the IBM 7 HP process**

<b>Metal layers</b>	<b>Design Width (<math>\mu\text{m}</math>)</b>	<b>Thickness (<math>\mu\text{m}</math>)</b>	<b><math>R_s</math> (<math>\Omega/\text{square}</math>)</b>
<b>M1, Mx, MT, x = 2, 3, 4</b>	$0.5 \leq M1 < 1.0$ $0.5 \leq Mx$	$0.36 \pm 0.05$	$0.07 \pm 0.012$
<b>M1, Mx, MT, x = 2, 3, 4</b>	$< 0.5$	$0.31 \pm 0.05$	$0.089 \pm 0.018$
<b>LY</b>	$\geq 1.52$	$1.25 \pm 0.13$	$0.023 \pm 0.005$
<b>AM</b>	$\geq 4.0$	$4.0 \pm 0.4$	$0.0070 \pm 0.0015$

First, the equivalent resistance ( $R_{eq}$ ) of the Basic Cell power rail can be calculated by Eq-4.1. If the width of the power rail is  $w$ ,  $R_{eq}$  will equal to  $1.225/w \Omega$ . Then  $R_{eq}$  is applied to a simplified power droop model as illustrated in Figure 4.22. In the FPGA, there are 16 BCs in each row and column. Each one is designed to have 1 mA currents flowing in it. Therefore, the  $R_1$  to  $R_{20}$  equal to  $R_{eq}$  and  $I_1$  to  $I_{16}$  equal to 22 mA. Applying those parameters to the model shown in Figure 4.22 and Eq-4.2, the width of the power rails should be more than  $68\mu\text{m}$ . To get less power droop on the rail,  $75\mu\text{m}$  is selected for the width in the FPGA core. Figure 4.23 shows the power rails in the Basic Cell.

**Table 4.3 Equations for calculating power droop and power rail width.**

$R_{eq} = \left(\frac{\rho}{t}\right) \times_s \left(\frac{l}{w}\right) = 0.007 \left(\frac{175}{w}\right) = \frac{1.225}{w} \Omega$	$\rho$ = resistivity $t$ = thickness $l$ = conductor length, $w$ = conductor width $R_{eq}$ = the sheet resistance ( $\Omega/\text{square}$ )
$V_A = 2.8 - 2.79 = (I_{20} + I_{19} + \dots + I_2 + I_1) \times 2R_1$ $+ (I_{20} + I_{19} + \dots + I_2) \times 2R_2 + \dots + (I_{20} + I_{19}) \times 2R_{19} + I_{20} \times 2R_{20}$	
Eq-4.1	
Eq-4.2	

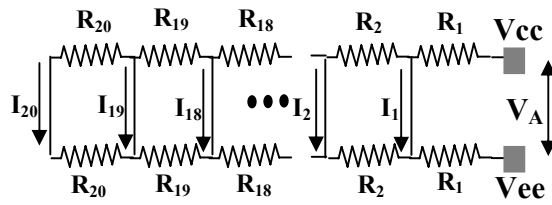


Figure 4.22 Simplified circuit model of the power distribution.

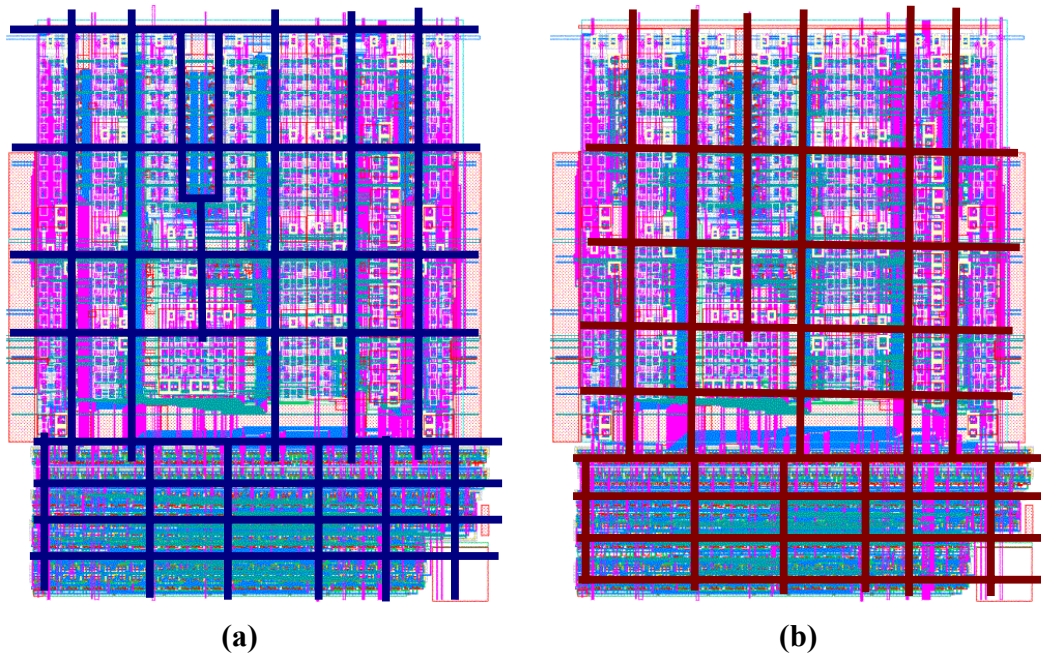


Figure 4.23 (a) Vcc (GND) power rail in the Basic Cell.. (b) Vee (-2.8 V) power rail of the Basic Cell.

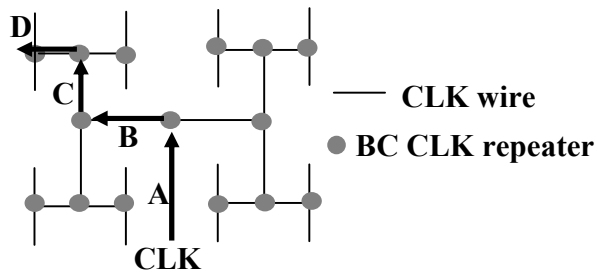
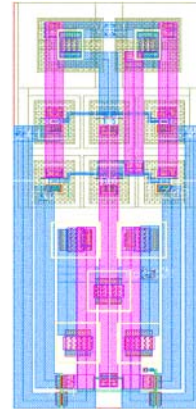
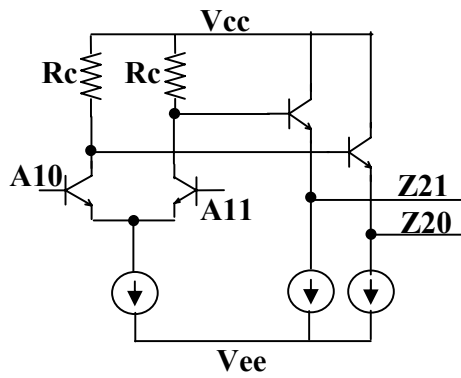


Figure 4.24 Clock tree of the 8x8 array as an example in the FPGA core.



(a)

(b)

**Figure 4.25 Schematic (a) and layout (b) of the clock repeater.**

#### 4.6 Clock and programming circuit clock distributions

To demonstrate the clock tree in the SiGe FPGA, an 8 x 8 BC array is used. The clock distribution shown in Figure 4.24 is based on the H-pattern structure which reduces the influence of parasitic effects and load effects to a minimum. Since the SiGe FPGA runs at higher frequency (in the GHz range), avoiding clock skew is very important. To alleviate the signal attenuation problem, repeaters are added to the clock tree. The schematic and layout of the repeater composed of a Current Mode Logic (CML) buffer and emitter followers are shown in Figure 4.25 (a) and (b). Figure 4.26 and 4.27 shows a test structure and simulation results of a clock repeater loaded with different length wires (400  $\mu\text{m}$  ~ 700  $\mu\text{m}$ ). One can observe that the output waveform of the 700  $\mu\text{m}$  wire case starts to distort. Therefore, the clock repeater can deliver the signals through a 700  $\mu\text{m}$  wire (when the input signal frequency is at 10 GHz). Figure 4.26 shows the simulated waveforms of the repeater outputs loaded with one to five repeaters. As more repeaters are added, the increase in the rise time is observed. Therefore, in the 20 x 20 FPGA, every repeater is loaded with only one repeater. Figure 4.28 shows the post layout simulation result of the partial tree from point A through B and C to D (The length of A, B, C, and D are 620, 360, 175 and 175  $\mu\text{m}$ ). In the same figure, the

propagation delay between point A and D is 30.6 ps. The layout of the programming circuit clock also follows the design methodology of the clock tree.

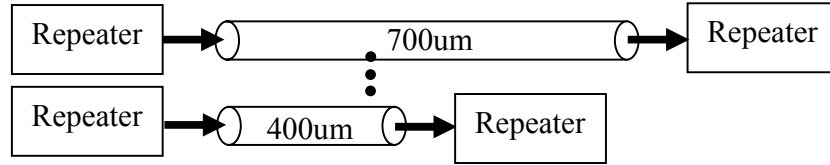


**Figure 4.26 Test structure of the repeater driving capability. The loaded wire is varied from 400~700 $\mu$ m.**

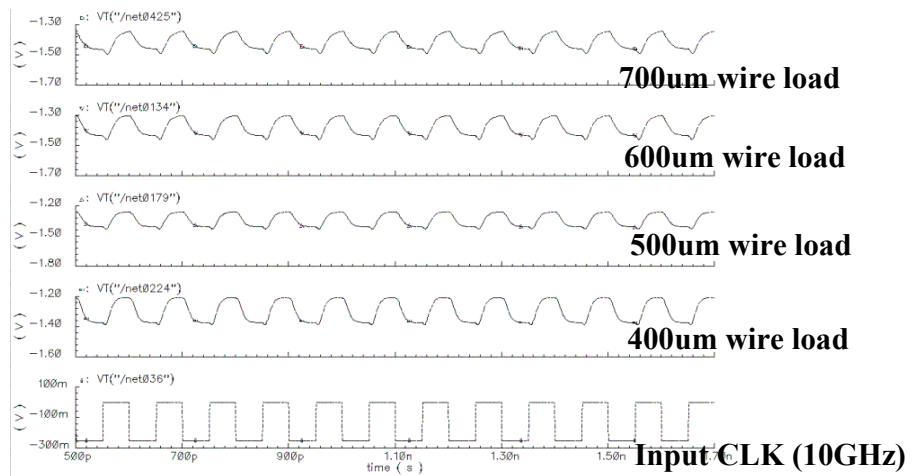


**Figure 4.27 Simulation result of the clock repeater driving 400~700 $\mu$ m wire loads with the 10 GHz test signal.**

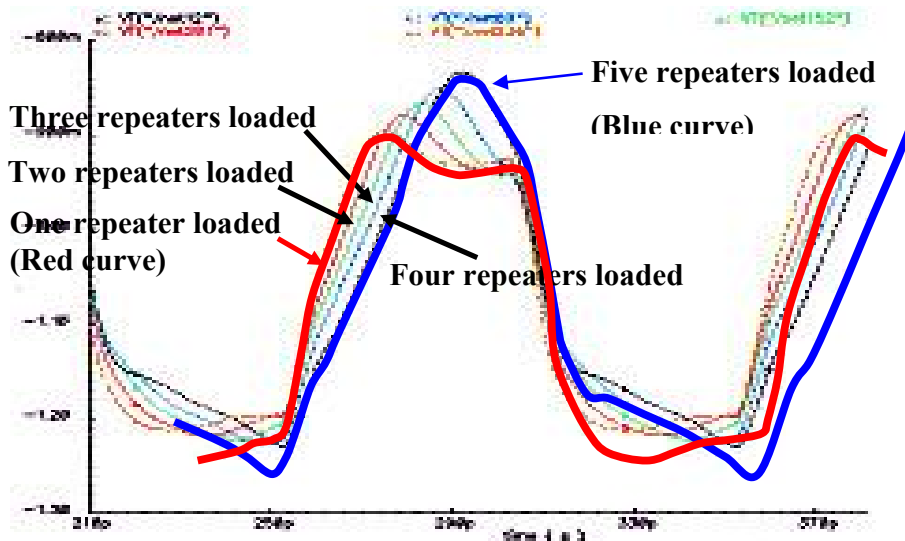


**Figure 4.28 Simulation result of the clock repeater loaded with one to five clock repeater loads.**

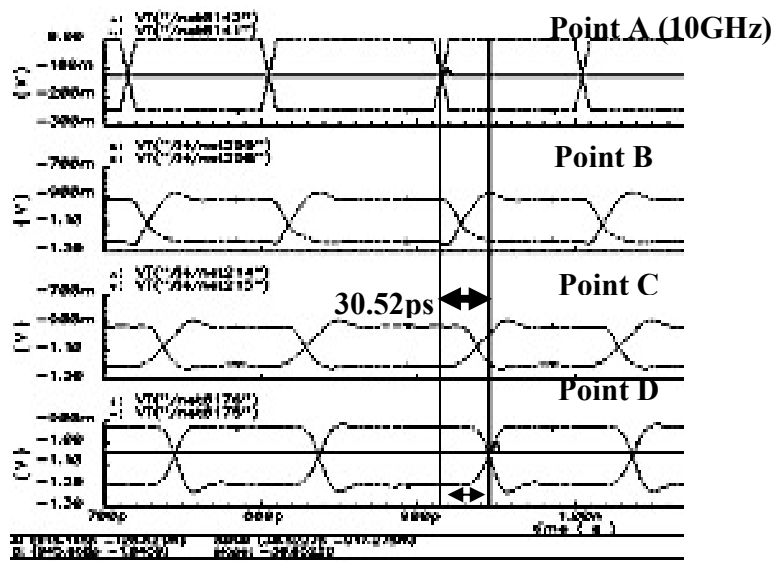


Figure 4.29 Propagation delay between A, B, C and D in clock tree shown in Figure 4.30

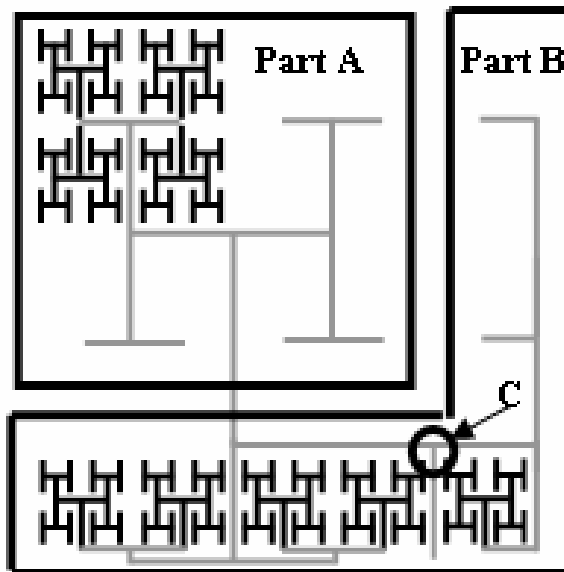
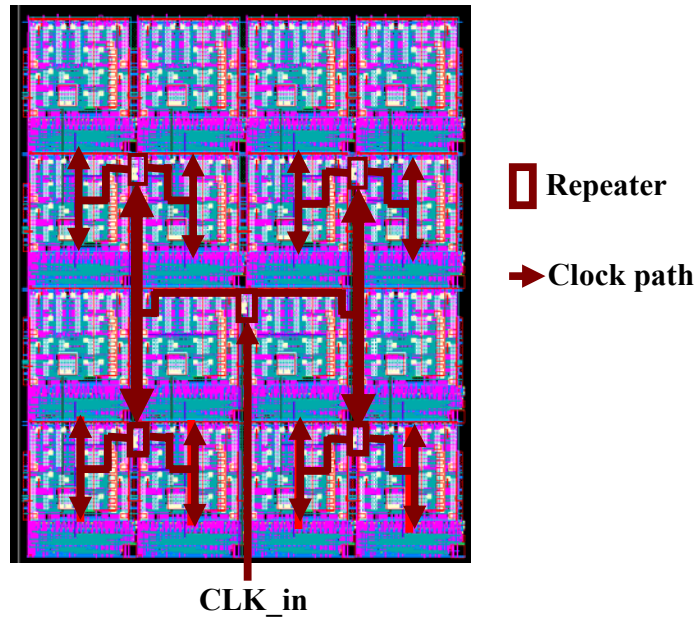


Figure 4.30 Clock distribution of the SiGe FPGA



**Figure 4.31 Detail clock distribution circuit in the 4 x 4 BC array.**

To minimize the clock skew of the clock tree, the delays in the clock tree must be correctly matched. This is usually accomplished by matching the driver and transmission line delays in each stage. Since this chip uses CML as the building logic, its differential nature suppresses induced phase noise. Therefore, the H-tree structure is adopted. Figure 4.30 shows the clock distribution of the SiGe FPGA. The clock distribution also uses differential signaling to avoid introducing cross talk between wires and phase noise. It is separated into two parts shown in Figure 4.30. Part A is the symmetric part (16 x 16 Basic Cell array). Part B is the asymmetric part. Since the FPGA repeatedly uses the same reconfigurable cell (Basic Cell), the load of each terminal at the end of the clock tree in part A is the same. Figure 4.30 shows the clock tree in the 4 x 4 BC array. In the clock distribution tree, all paths are designed to have the same length in order to have the clock signal arrive at every BC at the same time. Regarding Part B, it has an asymmetric layout which makes it more difficult to match the length of interconnects all the same, though each net has identical loads. Therefore, its layout should be designed more carefully. The method which tries to match the length of wires was used.

## 4.7 SiGe FPGA Basic Cell Configuration

The detailed data stream of the basic cell is described in this part. Then the data stream of the SiGe FPGA is mentioned. Figure 4.31 shows the schematic of the BC. It is separated into three parts. For each stage, input routing stage, configuration logic block and output routing stage, the configuration is explained. Table 4.4 lists the function table of the BCII which is the same with XC 6200 FPGA. First, the configuration of the input routing stage is described.

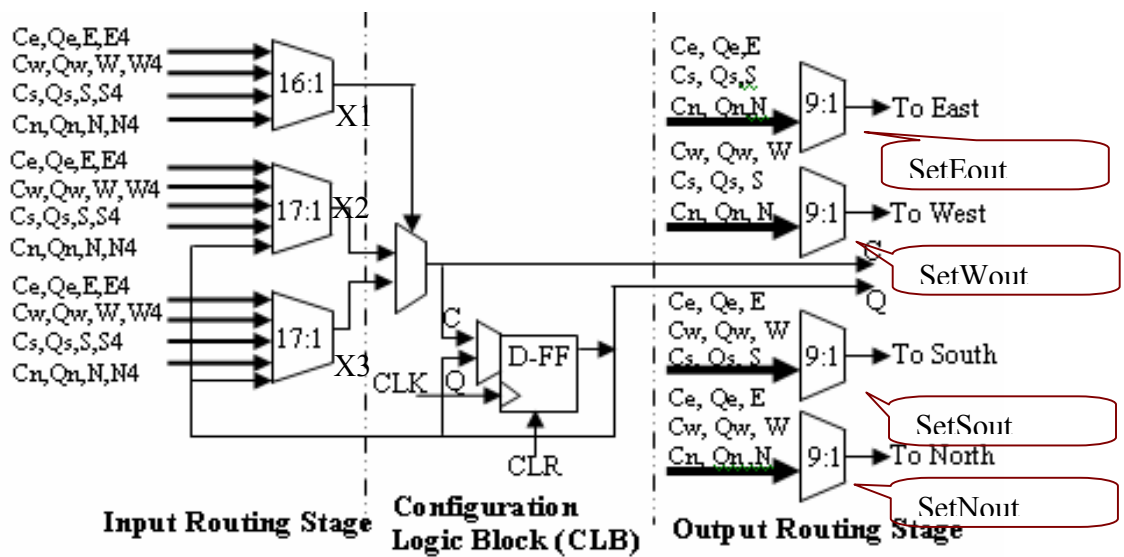
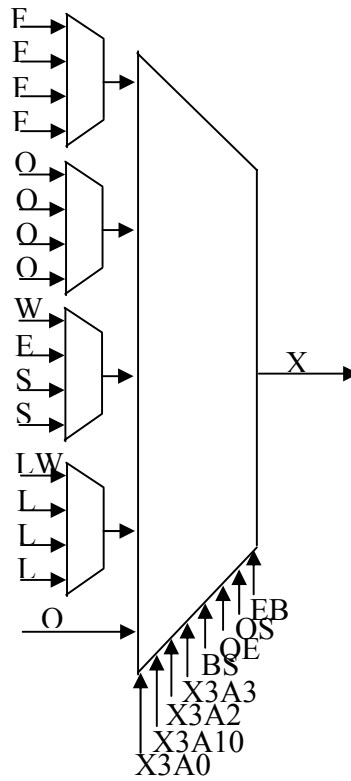


Figure 4.32 Schematic of the BCII.

Figure 4.32 shows the schematic of the MUX used in the Input Routing Stage. The configuration the MUXs are listed in Table 4.4~4.8. Table 21 lists the input signals of the Input Routing Stage. Table 4.4 shows the configuration of the MUXs. Figure 4.33 shows the Output Routing Stage. Table 4.5 and 4.6 show the input selection of the combinational and sequential logic functions and Table 4.7 shows the configuration of the output signals. Table 4.8 shows the bit arrangement of a BC.

**Input MUX configuration**



**Figure 4.33 Schematic of the MUXs in the input routing stage of a BC.**

**Table 4.4 Control signals of the input MUX**

Control signals	Function
<b>BS</b>	Bar signal select
<b>OS</b>	Original signal select
<b>QB</b>	Sequential bar signal (Qbar) select
<b>QS</b>	Sequential signal (Q)
<b>QE</b>	Sequential enable signal select
<b>EB</b>	Enable all.

**Table 4.5 Configuration of the input MUX: X1, X2 and X3**

	X3A00	X3A10	X3A20	X3A30	X3ABS	X3AQS	X3AQE
<b>FW</b>	1	1	1	1	0	X	0
<b>FE</b>	0	1	1	1	0	X	0
<b>FS</b>	1	0	1	1	0	X	0
<b>FN</b>	0	0	1	1	0	X	0
<b>QW</b>	1	1	0	1	0	X	0
<b>QE</b>	0	1	0	1	0	X	0
<b>QS</b>	1	0	0	1	0	X	0
<b>QN</b>	0	0	0	1	0	X	0
<b>WW</b>	1	1	1	0	0	X	0
<b>EE</b>	0	1	1	0	0	X	0
<b>SS</b>	1	0	1	0	0	X	0
<b>NN</b>	0	0	1	0	0	X	0
<b>LW</b>	1	1	0	0	0	X	0
<b>LE</b>	0	1	0	0	0	X	0
<b>LS</b>	1	0	0	0	0	X	0
<b>LN</b>	0	0	0	0	0	X	0
<b>Output invert</b>	X	X	X	X	1	X	0
<b>Sequential input -Q</b>	X	X	X	X	X	0	1
<b>Sequential input -Qbar</b>	X	X	X	X	X	1	1

**Table 4.6 Selection of the combinational and sequential operations**

	P	Q
<b>Combinational logic select (CS_en)</b>	1	0
<b>Sequential logic select (QS_en)</b>	0	1

**Table 4.7 Selection of the CLB combinational or sequential outputs**

	Enable X direction F output (FZx)	Enable sequential outputs (QZx)
<b>CEnbX</b>	1	X
<b>QEnbX</b>	X	1

Note: X indicates the directions to the east (E), west (W), north (N) and south (S)

**Output MUX configuration**

SetXout [00, 03]

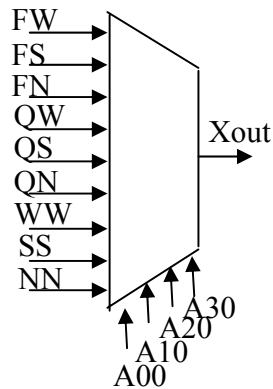


**Figure 4.34 Configuration of the MUX based in the Output Routing Stage.**

**Table 4.8 Configuration of the MUX of Output Routing Stage.**

	A00	A10	A20	A30
<b>FW</b>	1	1	1	0
<b>FS</b>	0	1	1	0
<b>FN</b>	1	0	1	0
<b>QW</b>	0	0	1	0
<b>QS</b>	1	1	0	0
<b>QN</b>	0	1	0	0
<b>WW</b>	1	0	0	0
<b>SS</b>	0	0	0	0
<b>NN</b>	1	1	1	1

Since the combinational and sequential outputs are directly routed to neighbor cells, the output MUX has been modified to handle the redirected signals. The setting of the redirected signals is listed in Table 4.9. For example, if a designer wants to select the input signal from the West (FW), the configuration bits for the Xout MUX must be set to 1110.

Table 4.9 shows the bit stream of the BCII. There are 42 configuration bits in the BC. Convenience for the layout of BC, the order of the bits has not been arranged to be in the sequence as listed in tables.

**Table 4.9 Bit pattern of the Basic Cell**

	0	1	2	3	4	5	6	7
<b>SRAM-out</b>	SetWout00	SetWout10	SetWout20	SetWout30	SetSout00	SetSout10	SetSout20	SetSout30
<b>SRAM-outb</b>	SetWout01	SetWout11	SetWout21	SetWout31	SetSout01	SetSout11	SetSout21	SetSout31
<b>Function</b>	Output MUX West setup				Output MUX South setup			

	8	9	10	11	12	13	14	15
<b>SRAM-out</b>	X2B00	X2B10	X2B20	X2B30	X2BBS	X3ABS	P	R
<b>SRAM-outb</b>	X2B01	X2B11	X2B21	X2B31	X2BOS	X3AOS	X	X
	Input Routing Stage X2 and X3 setup.						Combinational/ Sequential logic selection	

	16	17	18	19	20	21	22	23
<b>SRAM-out</b>	CEnbS	CEnbN	CEnbE	CEnbW	X3AQE	X2BQE	QEnb S	QEnbN
<b>SRAM-outb</b>	X	X	X	X	X	X	X	X
	Combinational output signals enable				X3 setup	X2 setup	Sequential output signals enable	

	24	25	26	27	28	29	30	31
<b>SRAM-out</b>	QEnbE	QEnbW	X3A30	X3A20	X3A10	X3A00	X1C00	X1C10
<b>SRAM-outb</b>	X	X	X3A31	X3A21	X3A11	X3A01	X1C01	X1C11
	Input Routing Stage X3 setup.							

	32	33	34	35	36	37	38
<b>SRAM-out</b>	X1C20	X1C30	SetEout30	SetEout20	SetEout10	SetEout00	SetNout30
<b>SRAM-outb</b>	X1C21	X1C31	SetEout31	SetEout21	SetEout11	SetEout01	SetNout31
	Input Routing Stage X1 setup.		Output Routing Stage output direction setup.				

	39	40	41
<b>SRAM-out</b>	SetNout20	SetNout10	SetNout00
<b>SRAM-outb</b>	SetNout21	SetNout11	SetNout01
	Contd.		

#### 4.8 Programming the Basic cell array

Basically, programming the 4 x 4 array is about the same as programming a single BCII. The only thing of note is the sequence of each BCII bit stream. Figure 4.35 shows the bit stream sequence of the 4 x 4 array. While programming the 4x4 array, the data stream is routed back from right to the left in the 2<sup>nd</sup> row of BCs after shifting through the 1<sup>st</sup> row of BCs from left to right. Following this route, the data stream routed to the 4<sup>th</sup> row will also be reversed.

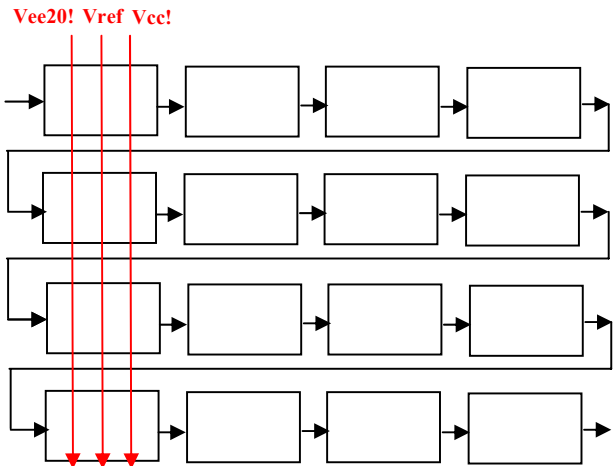


**Figure 4.35 Configuration data path in the 4x4 BC array**

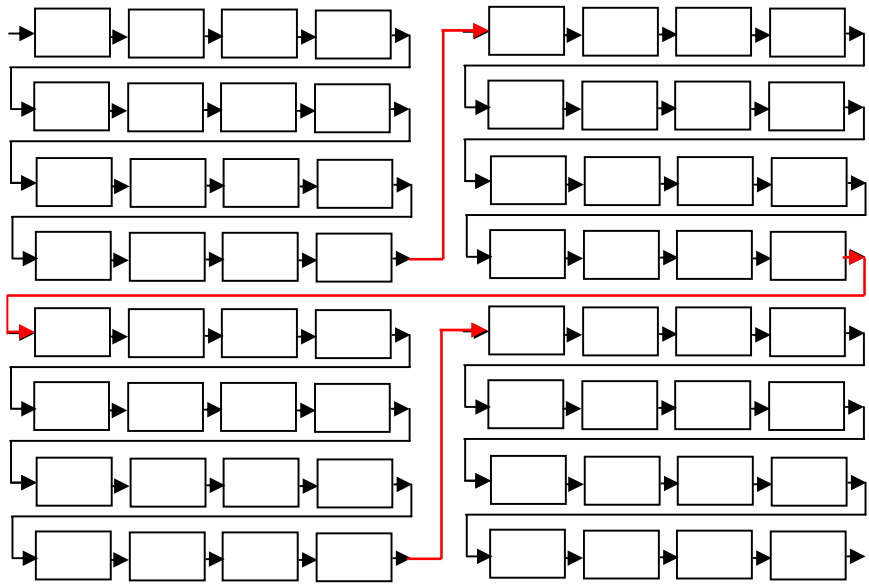


**Figure 4.36 Block diagram and data stream path of the 8 x 8 BC array.**

Fig. 4.37 is the schematic of the external programming circuit which was realized by an FPGA board. Lpm\_rom7 is the memory that stores all the data to be sent to the FPGA chip. There is also another circuit connecting the FPGA board to the FPGA chip to transfer the output voltage of the board from (0V, 5V) to (-2.8V, 0V). This circuit is realized by simple voltage dividers.

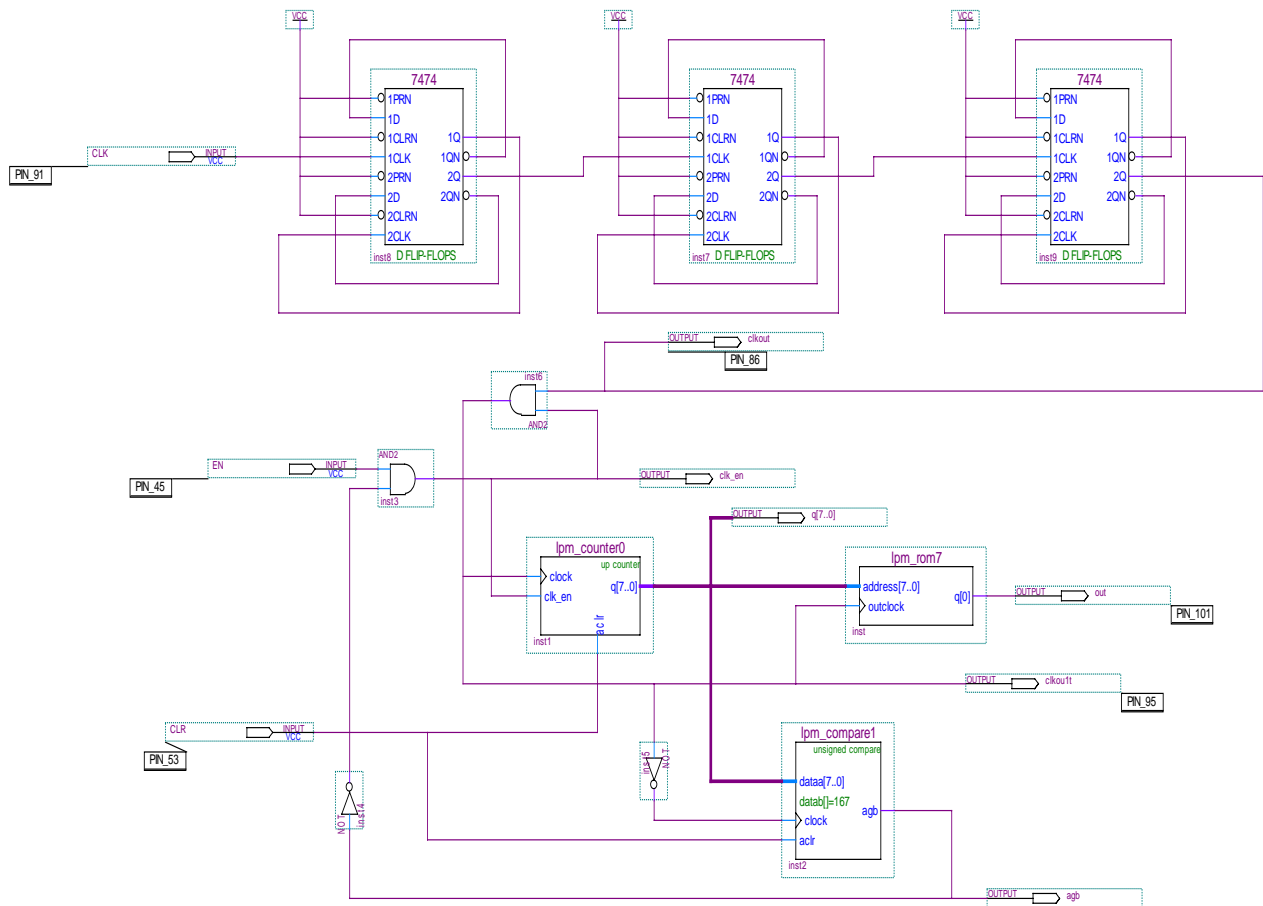


**Figure 4.37 Programming Circuit**

## 4.9 Pin assignments of the 16 x 16 FPGA

Figure 4.38 shows the pin arrangement of the new 16-pin probe. There are 4 low speed signal pins and 6 high speed pins. To avoid cross talk among the signals and from other noise sources, the high speed probes are placed between power pads. Figure 4.39 shows the power probe to deliver power to the 16 x 16 FPGA. It has 10 pins on it. Among them, there are 4 pairs of Vcc-Vee pins and 2 low speed signal pins on both ends. Each power pin can deliver 1A. The total current of each power probe can deliver 8A. Since there are two power probes, the total current delivering to the 16 x 16 FPGA is 16A. The detail specification of the test probes can be found in the [www.ggb.com](http://www.ggb.com). Figure 4.39 shows the final 16 x 16 FPGA layout with the power rails.

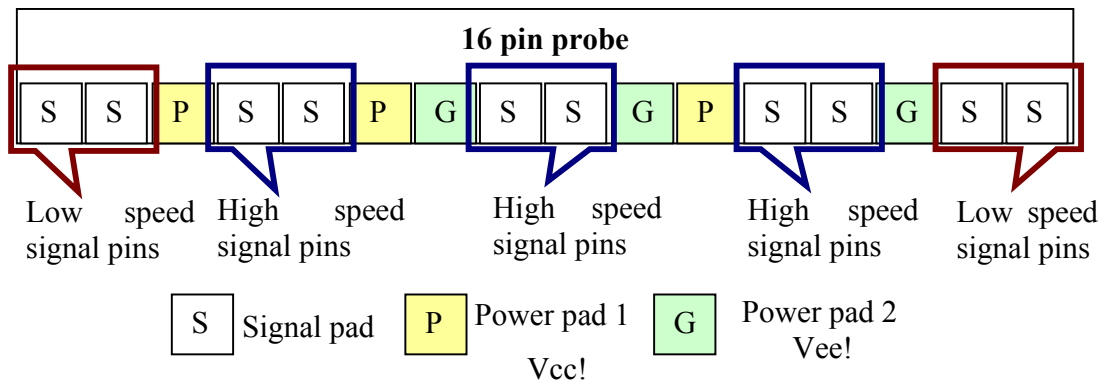


**Figure 4.38 Pin arrangement of the 16-pin probe used in the 16 x 16 SiGe FPGA.**

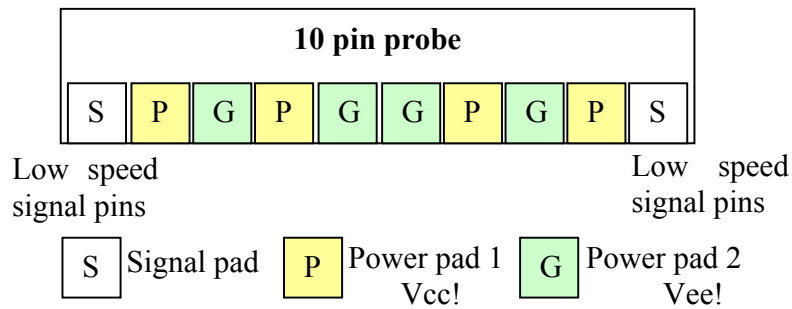


**Figure 4.39 Pin arrangement of the 10-pin power probe used in the 16 x 16 SiGe FPGA.**

#### 4.10 layout, programming sequence and power consumption

The layout of the SiGe 16 x 16 FPGA is shown in Figure 4.40. The center part is the 16 x 16 BC array, with two 10 pads and two 16 pads on four sides. The length of the chip is 2.85 mm x 3.8 mm.

Figure 4.41 shows the programming timing diagram. In the first cycle (Period A) the FPGA core is disabled by clearing the data left in the memory and shift register circuit to zero. Then the shift register starts to load the bit stream (Period B1). After

finishing shifting data, the Write-EN is activated and the data is loaded into the memory (Period B2). Then the FPGA starts to function by turning on the Read-EN (Period C). By using this scheme, the CMOS part and the bipolar will not be activated at the same time to avoid over driving the FPGA.

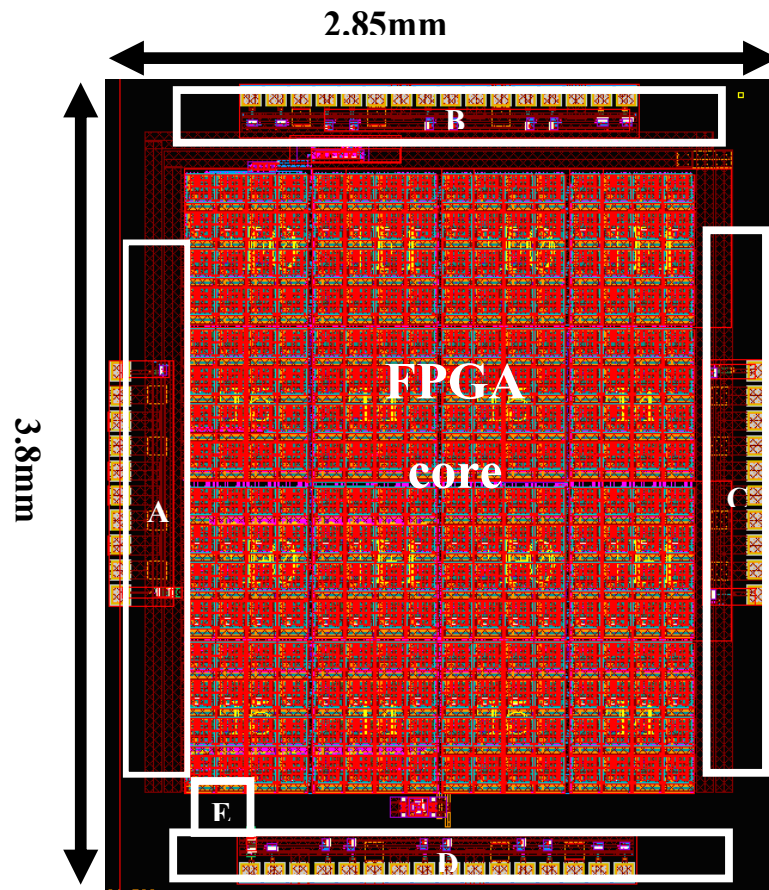


Figure 4.40 16 x 16 FPGA array programming structure



**A: Initialization period**

**B1: Programming bit stream period**

**B2: Loading bit stream period**

Figure 4.41 Timing diagram of the SiGe FPGA

This FPGA circuit is composed of CMOS and Bipolar parts. The CMOS logic is not consuming power when it reaches a stable state. The power dissipation of the CMOS is ignored here. Assuming all the current trees in the FPGA are turned on, the approximate power consumption can be calculated. The power consumption of subsections is also shown Table 4.10. Normally, when the FPGA is programmed, not all of the logic circuits perform functions. Based on the estimation and calculation described in Chapter 3, the least power consumption is 3.55 W. Other cases are also summarized in the same table.

**Table 4.10 Estimated power consumption of the different Basic Cell configurations**

Design		Usage	Estimated power consumption
BC Maximum Usage		100%	25 W
Case I (Comb./Sequential Logic)		47.6 % / 57.1%	11.9 W / 14.3 W
Case II	Sequential, One Redir.	71.4 %	17.9 W
	Sequential, Two Redir.	85.7 %	21.4 W
	Sequential, Three Redir.	100 %	25 W
Case III		14.2% / dir	3.6 W





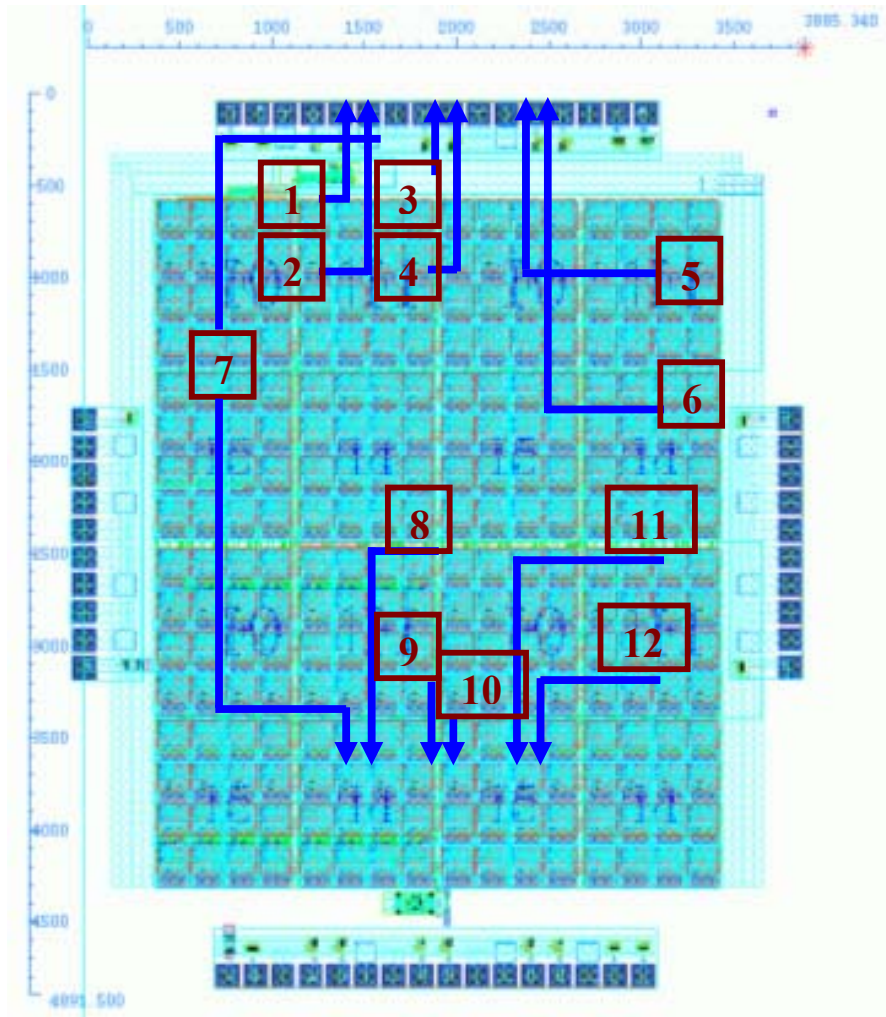


**Figure 5.4 Pin assignment of the high speed (> 10 GHz) signals.**

**1 and 2: Outputs of the first 4 x 4 array on the top-left corner.**

**3 and 4: Outputs of the top-left 8 x 8 array.**

**5 and 6: Outputs of the top-right 8 x 8 array.**

**7: Outputs of the LFSR trigger.**

**8 and 9: Outputs of the bottom-left 8 x 8 array.**

**10: Outputs of the VCO trigger ( $f_{VCO}/64$ ).**

**11 and 12: Outputs of the bottom-right 8 x 8 array.**

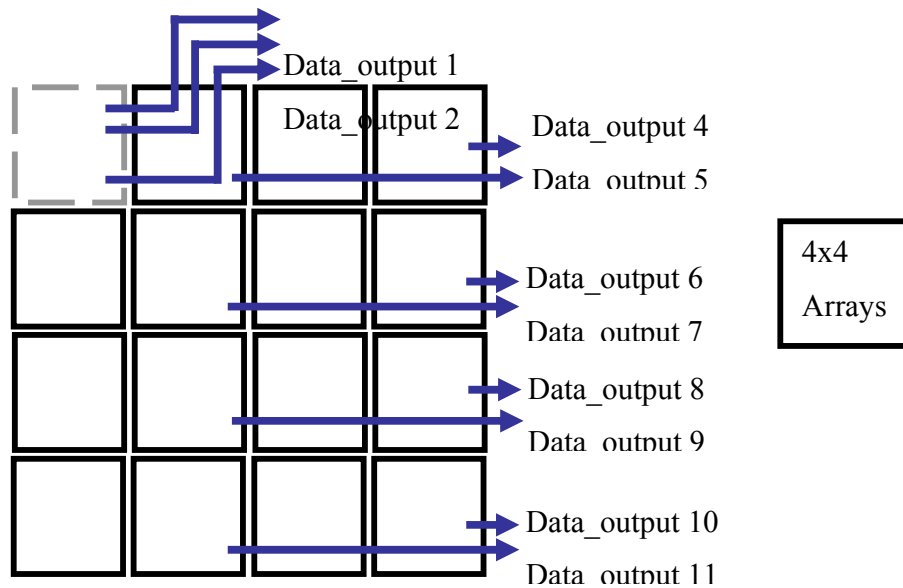


**Figure 5.5 Input / Output arrangement of the programming data.**

### 5.1.2 Test plan of the low speed part in the new FPGA

The main purpose of having the low signal test part is test the CMOS clock tree and programming circuits. Figure 5.4 shows the low speed signal test plan. The data outputs 1~11, of the 4 x 4 and 8 x 8 arrays are routed to the external pins to make sure the programming circuits work well. The tapered buffer is used to drive the output to the pins. In general, one can always add inverters to the end of a path without changing its function.

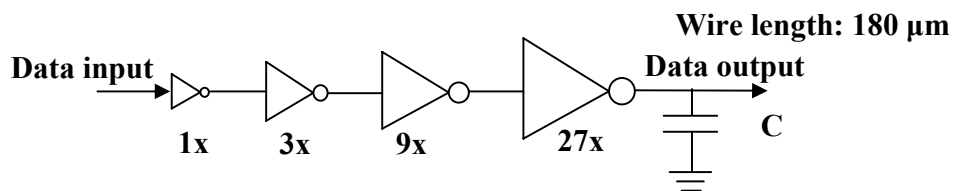


**Figure 5.6 Schematic of the tapered buffer driving a 180 μm wire**

the sizes of the inverters in the tapered buffer are incremented 4 times compared to its previous stage. Figure 5.6 shows the tapered buffer used in the data path of the

programming circuits. Figure 5.7 shows the pin assignment of the low speed signals of the 16 x 16 FPGA.

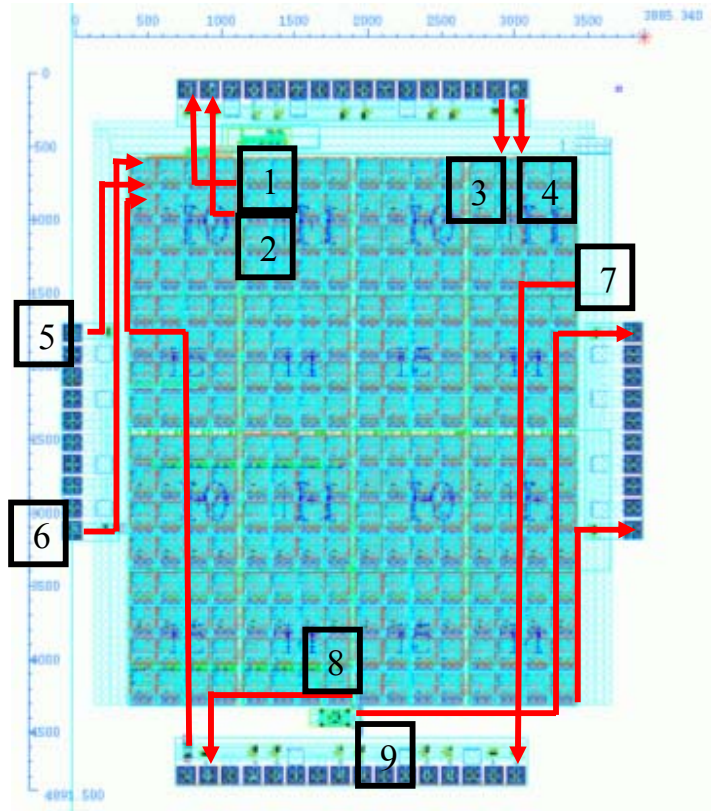


**Figure 5.7 Pin assignment of the low speed (> 1 GHz) inputs and outputs.**

- 1: Data output of the first two rows in the top-left 4 x 4 array.**
- 2: Data output of the second two row of BC in the top-left 4 x 4 array.**
- 3. Programming circuit: CLR**
- 4. Programming circuit: WR\_BAR.**
- 5. Data input.**
- 6. Low speed external input signal.**
- 7. Data output of the top-right 8 x 8 array.**
- 8. Data output of the bottom-right 8 x 8 array.**
- 9. CLK of the programming circuit.**

### 5.1.3 Test procedure

To test the CMOS programming circuits, a CMOS FPGA with memory programmed by its software can be used to generate the required signals. Figure 5.8

shows the test blocks that used in the SiGe FPGA test. The data stream of the SiGe FPGA can be generated before storing to the memory in the CMOS FPGA. The data stream is passed to the FIFO to synchronize with the CMOS\_CLK and shift out the data stream to the Data\_in of the programming circuits in SiGe FPGA.

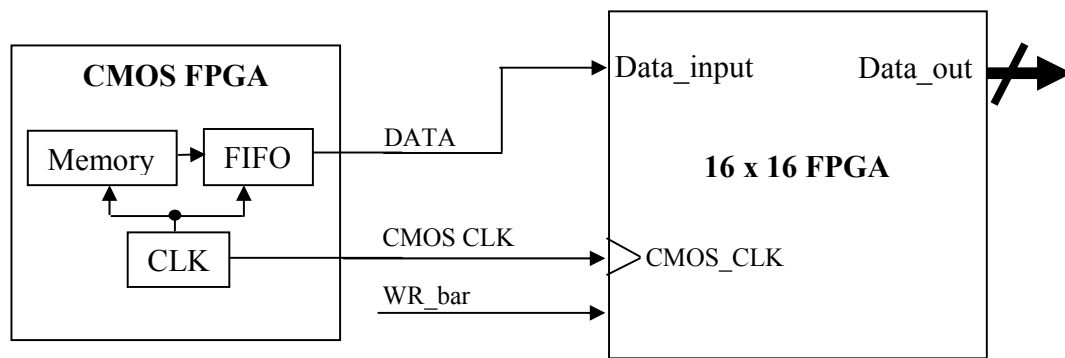


**Figure 5.9 Test blocks on programming the SiGe FPGA configuration with an FPGA board**

## 5.2 16 x 16 SiGe FPGA Test Results

The first several tests shows that global clock signal generated by the VCO is not transmitted to all the basic cells and LFSR correctly, which might be because the input resistance of the clock pin on each basic cell is not big enough and therefore lower the input signal voltage level. Now the test plans can not be executed on this chip.

However, the following tests show that the chip is still working well in the sequential mode.

### 1. 8-stage ring oscillator

To generate a clock signal, an 8-stage ring oscillator is constructed by programming 7 basic cells as bypass repeaters and 1 basic cell as an inverter (Fig. 5.10). Fig. 5.11 shows the frequency of the oscillator is 1.5273GHz.

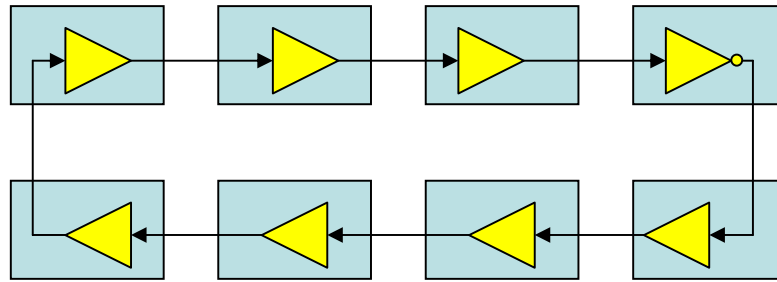


**Figure 5.10. 8-stage Ring Oscillator Test Circuitry**

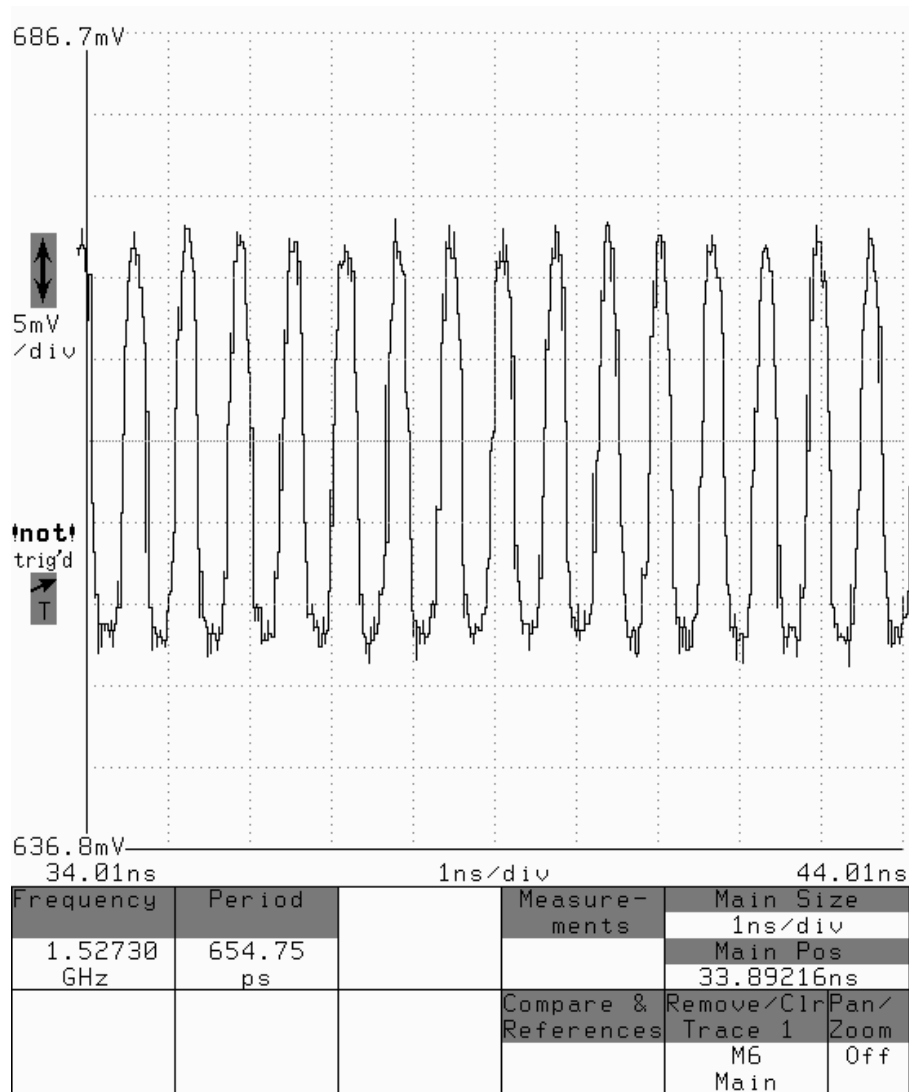


**Figure 5.11 8-stage Ring Oscillator Test Result**

The basic cells in the bypass repeater mode do not contain any logic part and therefore are the fastest units of this loop. The number of CML's used in an inverter ( or any other logic function) is twice of bypass repeaters, which means, the delay time cost in the inverter (or any logic function) can be estimated to be around twice of the delay time cost in the bypass repeater.

For the 8-oscillator loop, we have

$$2(7x + y) = 1/1.5273GHz \quad (1)$$

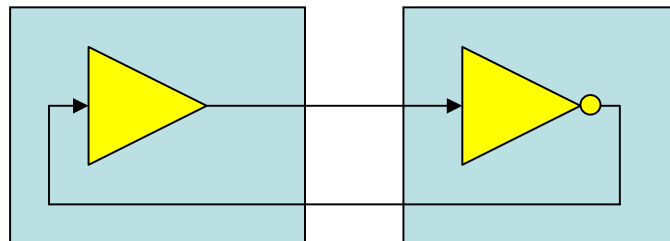
Where x is the time cost in the bypass repeater, and y is the time cost in the inverter.

## 2. 2-stage ring oscillator

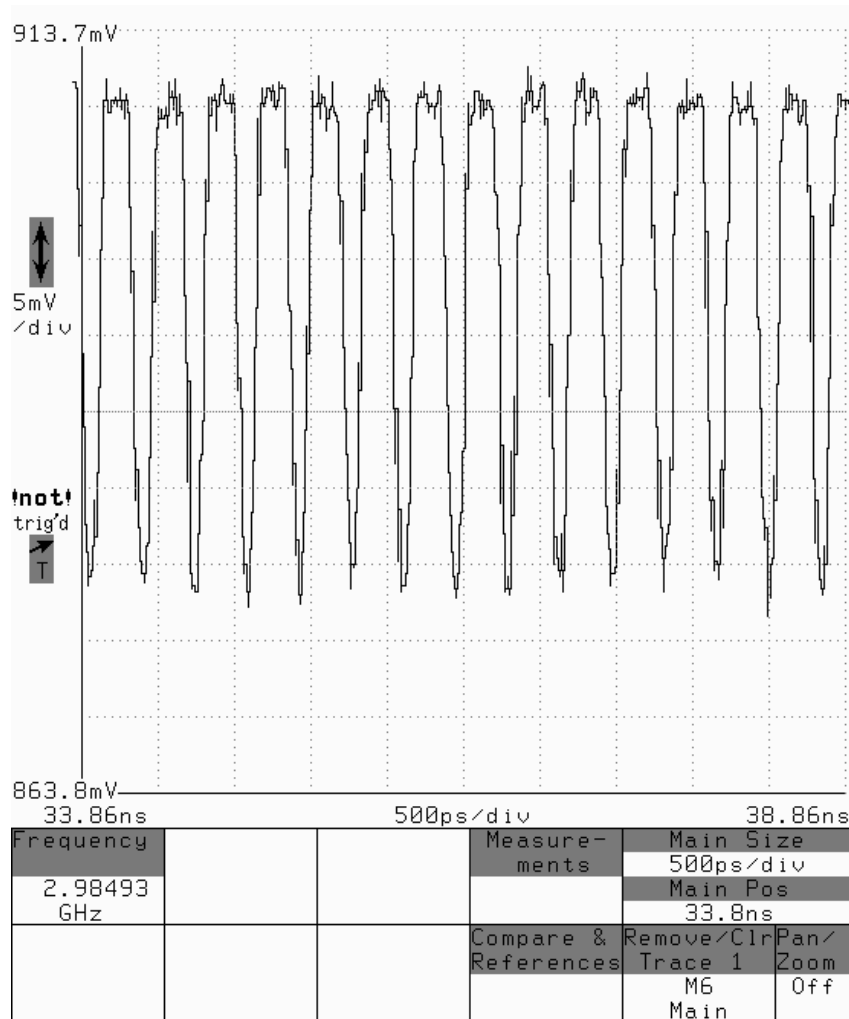
To find out x and y, a 2-stage ring oscillator is constructed by programming a repeater (not in bypass mode for the signal from a certain direction can not be transmitted in the bypass mode back to the same direction) and an inverter in a loop.

Fig.18 shows the frequency of the oscillator is 2.98493GHz. Then the second equation is

$$2(x + y) = 1/2.98GHz \quad (2)$$



**Figure 5.12. 2-stage Ring Oscillator Test circuitry**



**Figure 5.13 2-stage Ring Oscillator Test Result**

Solve equation (1) and (2), we have

$$x=34\text{ps, and }y=84\text{ps.}$$

Or,

$$1/x=28.76\text{GHz, and }1/y=11.94\text{Hz.}$$

The fact that repeater and inverter logic are realized successfully shows that the FPGA chip works as expected, since all other logic functions are configured in the same way. As a bypass repeater, a basic cell can work at up to 28.76GHz, and as any logic functions unit, such as MUX, XOR, etc, it can run up to 11.94GHz.

### 5.3 The New 16 x 16 FPGA chip design

The 16 x 16 FPGA chip tested was designed by Dr. Jong-ru Guo at the end of 2005. It was the first working FPGA chip of this project, while it still has several shortcomings:

1. Vdd is supplied by positive voltage, which adds more noise to the circuit.
2. The buffer used between each two basic cell memories is an inverter, which converts the polarity of the data.
3. There is no high speed input signal.
4. There is no external clock signal.
5. LFSR is too long from the VCO, which might be the reason that LFSR doesn't work.

The author fixed these problems by doing the following updates:

1. Switch the pads of power and ground, including the power and ground rails inside the chip.
2. Add another inverter between each two basic cells' memories to make it a buffer.
3. Change the two input (X1 and X2) to the high speed pad.
4. Change one of the high speed output pad to an external clock signal input.
5. Setup an internal oscillator by using one basic cell's bypass mode, which can be used as a high speed internal signal.

Now this new 16 x 16 chip has already been fabricated, and will be ready to test.

### 5.4 Future work

To get higher goal of the project, the following acts can be made in the future:

1. Move the whole design into 8HP or even 9HP technology, which will cost less power and get higher frequency.
2. Add switches in each Basic Cell to show down those non-working basic cells, so that the power consumption will be decreased farther.

3. Fig. 2.8 and Table 2.2 show that one basic cell can't perform a simple NAND logic, but AND is working well. So adding another bit to determine whether to convert the polarity of the output will solve this problem.

## References

- [1] Michael John and Sebastian Smith, "Application-Specific Integrated Circuits", Addison-Wesley VLSI System Series
- [2] John F. McDonald et al, "Reconfigurable FPGA's in the 1-20 GHz Bandwidth with HBT BiCMOS", Proceedings of the first NASA/ DoD Workshop on Evolvable Hardware
- [3] Bryan Goda et al, "SiGe HBT BiCMOS FPGAs for high speed reconfigurable computing" IEE Proc. Computer and Digital Technology, vol 147. NO.3, May 2000
- [4] Jong-ru, Guo, "A 16X16 Basic-Cell High Speed Silicon Germanium Field Programmable Gate Array", Ph.D. Thesis, Rensselaer Polytechnic Institute, Oct. 2005
- [5] John D. Cressler, "SiGe HBT Technology: A New Contender for Si-Based RF and Microwave Circuit Applications", IEEE Tran. on Microwave Theory and Techniques, VOL. 46, NO. 5, May, 1998.
- [6] Flash Comm. [www.flashcomm.com](http://www.flashcomm.com).
- [7] IEEE spectrum SiGe cross section figure.
- [8] Okan Erdogan, "A Three-Port Pipelined Register File Implemented Using a SiGe HBT BiCMOS Technology", Ph.D. Thesis, Rensselaer Polytechnic Institute, Dec 2006
- [9] Chao You, "A High-Speed, Low Power SiGe BiCMOS FPGA with New Features for Applications", Ph.D. Thesis, Rensselaer Polytechnic Institute, May 2005
- [10] Kuan Zhou, "LOW-POWER MULTI-GHZ SIGE FPGAS FOR RECONFIGURABLE COMPUTING", Ph.D. Thesis, Rensselaer Polytechnic Institute, July 2004
- [11] Raminderpal Singh, David L Hareme and Modest M. Oprysko. "Silicon Germanium Technology, Modeling and Design". IEEE press
- [12] D. Lammer, "IBM SiGe hits 350 GHz", Microwave Engineering, [www.mwee.com/mweenews/showsarticle](http://www.mwee.com/mweenews/showsarticle), Nov 02, 2002.
- [13] Greg Freeman et al, "40 Gb/s Circuits Built from a 120 GHz fT SiGe Technology", IEEE Journal of Solid State Circuits, vol. 9. September, 2002
- [14] Y. Taur and T. H. Ning, "Fundamentals of Modern VLSI Devices", Cambridge University Press, 1998

- [15] John D. Cressler, "SiGe HBT Technology: A New Contender for Si-Based RF and Microwave Circuit Applications", IEEE Tran. on Microwave Theory and Techniques, VOL. 46, NO. 5, May, 1998
- [16] D. L. Hareme, et al "Current Status and Future Trends of SiGe BiCMOS Technology" IEEE Trans. On Electron Device, VOL. 48, NO. 11, Novemember, 2001
- [17] J. Sitch, et al, "HBT IC's for OC-192 equipments", Int. J. High Speed Electron System, Special Issue on High Speed Circuits for Light wave Communications, K. C. Wang, Ed., 1999
- [18] Ken Martin, "Digital Integrated Circuit Design", Oxford University Press Inc.
- [19] Kiyoshi Ishii et al, "4-bit Multiplexer/Demultiplexer Chip Set for 40-Gbit/s Optical Communication Systems" IEEE Trans. On Microwave Theory and Techniques, VOL. 51, NO. 11, 2003.
- [20] Samuel A. Steidl, " A 32-Word by 32-bit Three-port Bipolar Register File Implemented Using a SiGe HBT BiCMOS Technology", Ph.D. Thesis, Rensselaer Polytechnic Institute, May 2001
- [21] XC6200 data sheet.
- [22] Keiji Kishine et al, "A High Speed, Low-Power Bipolar Digital Circuit for Gb/s LSI's: Current Mirror Control Logic", IEEE Journal of Solid State Circuits, Vol.32 No. 2, Februrary, 1997
- [23] Gerd Schuppener, et al, "Investigation on Low-Voltage, Low Power Silicon Bipolar Topology High Speed Digital Circuits", IEEE Journal of Solid State Circuits, Vol. 35, No. 7, July 2000
- [24] Xilinx Power consumption work sheet V 1.5, <http://www.xilinx.com/cgi-bin/powerweb.pl>.
- [25] T. W. Krawczyk, et al, "SiGe HBT serial transmitter architecture for high speed variable bit rate intercomputer networking", IEE Proc. Circuits Devices Syst.
- [26] IBM 7HP design manual.
- [27] G. Freeman et al. "40 Gb/s Circuits Built From a 120-GHz fT SiGe Technology" IEEE Journal of Solid-State Circuits, Vol. 37, NO. 9, 2002, pp1106-1114.
- [28] Behzad Razavi 'Design of Integrated Circuits for Optical Communications', pp12~14, McGraw-Hill, 2003.

- [29] Anatha Chandrakasan, William J. Bowhill and Frank Fox. "Design of high-performance Microprocessor Circuits", IEEE Press
- [30] Self test text book.
- [31] Jong-Ru Guo, et, al, "A high speed Reconfigurable Gate Array for Gigahertz Applications", Annual Symposium on VLSI, p 124~129. May, 2005
- [32] Xilinx Virtex data sheet.
- [33] Xilinx Power consumption work sheet V 1.5, <http://www.xilinx.com/cgi-bin/powerweb.pl>.
- [34] Cadence design manual, "Diva Product Notes"
- [35] Neil H. E. Weste, David Harris, "CMOS VLSI DESIGN", Pearson Education Inc.
- [36]. Ralph Niederberger, et al. "High speed Supercomputer communications in Broadband Networks"